arXiv:2609.06272v1 [cs.SE] 5 Sep 2026

KG-Commit: A Dynamic Knowledge Graph for Online Just-in-Time Software Defect Prediction

Mohsen Hesamolhokama[a], Mohammad Sina Beyrami Aghbash[a], Behnam Rohani[b], Mohammadamin Fazli[a], Jafar Habibi[a]

[a]*Department of Computer Engineering, Sharif University of Technology, Tehran, Iran*
[b]*Department of Mathematical Sciences, Sharif University of Technology, Tehran, Iran*

Abstract

Just-in-time software defect prediction (JIT-SDP) aims to identify risky commits as they arrive and provide developers with timely feedback. This need for low latency has led most approaches to rely on commit-level information and overlook the broader project context in which a change occurs. Incorporating this context is challenging because it requires both efficient retrieval for incoming commits and continual maintenance as the repository evolves. We introduce KG-Commit, a dynamic knowledge graph that incrementally maintains repository history, within-file code structure, and commit semantics as the project evolves. It also uses an AST-delta mechanism to track structural changes between file edits and relies on lightweight graph inference running entirely on CPU. Our evaluation on 11 Apache software projects against six baselines shows that KG-Commit achieves the highest aggregate Macro-F1 (0.704), G-Mean (0.706), and AUC (0.809) using our selected inference pipeline. Under a realistic online protocol, it outperforms LR, HGB, RF, and DeepJIT on all 11 projects, LApredict on 10, and JITLine on 9 projects in Macro-F1, with the aggregate paired difference significant in every case. KG-Commit processes each commit in approximately 1.33 s, with a cost that remains stable as the graph grows and is compatible with commit rates observed in real-world projects. These findings show that rich project context can be efficiently maintained and exploited for online JIT-SDP.

Keywords: Online Defect Prediction, Knowledge Graph, Just-in-Time, Real-time Project Evolution

1. Introduction

Software underpins nearly every product and service that people rely on, and even a single defect can disrupt a critical system. Ensuring software quality is therefore a persistent concern for development teams, yet the time and resources available for testing and code review are limited. Software defect prediction (SDP) helps teams direct that effort to the right place by estimating which parts of a system are most likely to be faulty (Menzies et al., 2007; Lessmann et al., 2008; Hall et al., 2012). Traditional SDP approaches operate at the level of files, modules, or releases (Wang et al., 2016; Li et al., 2017; Zhou et al., 2022). At this granularity, predictions often arrive only after many changes have accumulated, making it difficult to identify the particular change that introduced a defect and to recover the context in which it was made. Just-in-time defect prediction (JIT-SDP) was introduced to close this gap (Mockus and Weiss, 2000; Kamei et al., 2013). It evaluates each commit as soon as it is submitted, so a risky change can be reviewed while its author still remembers the context. Because of this immediate feedback, JIT-SDP has become a natural fit for continuous integration and an active research topic (Zhao et al., 2023).

For more than a decade, JIT-SDP has relied primarily on a compact set of hand-crafted metrics that summarize each commit. These metrics capture properties such as change size, code churn (Nagappan and Ball, 2005), the extent to which a change spans files and subsystems, and the experience of its author (Kamei et al., 2013; McIntosh and Kamei, 2018). Standard classifiers then use these summaries to estimate defect risk. As deep learning became more prominent, research gradually shifted from hand-crafted commit features to deep representation learning. Yang et al. (2015b) used

Email addresses: hokama@ce.sharif.edu (Mohsen Hesamolhokama), sina.beirami@sharif.edu (Mohammad Sina Beyrami Aghbash), behnam.rohani058@sharif.edu (Behnam Rohani), fazli@sharif.edu (Mohammadamin Fazli), jhabibi@sharif.edu (Jafar Habibi)

a deep belief network to transform conventional metrics into richer features, while DeepJIT and CC2Vec learned representations from commit messages and code diffs (Hoang et al., 2019, 2020). Later work extended this direction with line-level defect localization (Pornprasit and Tantithamthavorn, 2021, 2023), pre-trained code encoders such as CodeBERT (Ni et al., 2022; Jiang et al., 2025), and parameter-efficient adaptation of these models (Abu Talib et al., 2024).

What these models largely overlook is the broader project context in which the change occurs (Bryan and Moriano, 2023; Zhao et al., 2023). Knowledge graphs are well suited to representing such structure because they organize information as entities connected by typed relations (Hogan et al., 2021; Ji et al., 2022) and support reasoning and learning over these relations (Nickel et al., 2016). They have been applied successfully in areas such as recommendation, life sciences, and cybersecurity (Wang et al., 2019; MacLean, 2021; Zhao et al., 2024). Their use in software engineering, however, remains relatively limited and has focused mainly on organizing software artifacts such as APIs and libraries (Liu et al., 2023b). Knowledge graphs remain even less explored in software defect prediction and, to the best of our knowledge, have not been applied to JIT-SDP. This gap is particularly notable because a commit is inherently relational. It modifies specific files and functions, interacts with other parts of the system, is associated with an author, and carries an intent expressed through its message. Dynamic knowledge graphs provide a natural way to capture these evolving relationships (Zhang et al., 2024; Cai et al., 2024). By incorporating new events as they occur, they maintain an up-to-date representation of a changing domain (Trivedi et al., 2017; Goel et al., 2020). Since software evolves incrementally through a stream of commits, this representation is especially well aligned with the online nature of JIT-SDP.

In just-in-time prediction, however, accuracy is of little value if it arrives too late (Kamei et al., 2013), so richer context must be incorporated at a computational cost that remains practical for an incoming stream of commits. This creates a tension between contextual richness and per-commit processing cost. Project-level context, such as how a changed function is called elsewhere or how a file depends on others, is known to improve defect prediction (Zimmermann et al., 2009; Nam et al., 2013), but reconstructing this information from scratch for every incoming commit can be expensive. To remain efficient, many approaches mainly rely on information contained within the commit itself, such as its message and code diff (Hoang et al., 2019, 2020; Pornprasit and Tantithamthavorn, 2021). Others pursue efficiency more aggressively through a single inexpensive feature (Zeng et al., 2021) or lightweight retrieval over historical commits (Sahar et al., 2024). The open question is whether rich, project-specific context can be maintained at a cost compatible with the pace at which commits actually arrive.

Dynamic or real-time knowledge graphs offer a natural way to address this problem. Rather than reconstructing the project state from scratch, the graph is updated incrementally as each commit arrives, with each update affecting only the relevant portion of the graph (Zhao and Chen, 2023). The accumulated project context can then be queried through a graph query language such as Cypher (Francis et al., 2018; Angles et al., 2017). This replaces repeated reconstruction of project history with incremental per-commit work. Its practical suitability therefore depends on whether this processing cost remains stable as the project grows and is sufficiently small relative to the rate at which commits arrive.

Building on this idea, we introduce KG-Commit, a dynamic knowledge graph that evolves with the repository and provides project-specific context at inference time. KG-Commit is maintained incrementally in Neo4j and organizes information across three layers: (1) Core layer for repository entities and their relations, (2) AST layer for within-file program structure, and (3) Commit Semantic-Text Graph (CSTG) layer for the semantics of commit messages and code changes. We combine graph-based and feature-based inference over these representations to estimate defect risk and evaluate KG-Commit in terms of predictive performance, query and update cost, and suitability for online JIT-SDP.

1.1. Motivating Example

Consider a commit that only moves a file, for example relocating `Config.java` from the `com.app.utils` package to `com.app.core` (Figure 1). Judged on its own, the commit looks harmless. It moves a file without changing its contents, so its change metrics are small and nothing inside the change points to a defect. A developer reviewing only the change, or a model that relies only on commit-level information, would therefore be likely to classify it as clean (Hoang et al., 2019; Zeng et al., 2021). The commit is nonetheless bug-inducing, because another part of the project still refers to the file through its old package. The file `ApiServer.java`, which this commit does not touch, still contains `import com.app.utils.Config;`. After the move, this import refers to a class that no longer exists in that package, causing the build to fail. This defect cannot be de-

tected from the commit in isolation. It becomes visible only when the rest of the project is taken into account. Reliably labeling such a commit therefore requires information about the project context that surrounds the change.

Figure 1: A commit moves `Config.java` from package `com.app.utils` to `com.app.core`. The change has no effect inside the file, so it looks clean, but `ApiServer.java` elsewhere in the project still imports `com.app.utils.Config` and fails to compile. The defect is not visible from the commit alone.

1.2. Contributions

The main contributions of this paper are as follows:

- **A Practical Solution to Rich Project Context in Online JIT-SDP.** KG-Commit addresses the difficulty of incorporating rich project context without sacrificing the speed required for JIT-SDP. To the best of our knowledge, it is the first knowledge graph designed for JIT-SDP. It represents repository history, code structure, and commit semantics in a Neo4j graph database.
- **Incremental Maintenance of Within-File Structure through AST Deltas.** We introduce an AST-delta mechanism that tracks how a file's structure changes between edits by recording added, removed, updated, and moved AST nodes. This lets KG-Commit maintain fine-grained within-file structure incrementally as the project evolves.
- **Strong Predictive Performance with Efficient and Scalable Deployment.** KG-Commit achieves the highest aggregate Macro-F1, G-Mean, and AUC against six baselines across 11 real-world projects under a fixed online protocol. It outperforms each baseline on at least 9 out of the 11 projects in Macro-F1, with statistically significant aggregate differences against all of them. KG-Commit processes each incoming commit in approximately 1.33 s on CPU. Lifecycle analysis further shows that per-commit processing remains stable as the graph grows, supporting the practical use of KG-Commit throughout project evolution.

1.3. Paper Outline

The remainder of this paper is organized as follows. Section 2 reviews related work on JIT-SDP, code representation, and knowledge graphs. Section 3 presents KG-Commit, its layered representation, incremental maintenance, and inference methods. Section 4 describes the experimental design and online evaluation protocol. Section 5 reports predictive performance, efficiency and scalability, layer contributions, and inference-channel analysis. Section 6 discusses the main findings, deployment considerations, sensitivity to operational constraints, limitations, and future work. Section 7 addresses threats to validity, and Section 8 concludes the paper.

2. Related Work

Our work brings together three research lines: JIT-SDP, the representation of source code for defect prediction, and knowledge graphs. We review each line in turn and close by positioning our proposal, which represents the sequence of code changes as a dynamic knowledge graph and queries that graph to predict defects.

2.1. Just-in-Time Software Defect Prediction

Traditional defect prediction works at coarse levels such as the file, module, or the release (Menzies et al., 2010). This approach delays feedback and forces developers to inspect large amounts of code. More recently, Hesamolhokama et al. (2025) showed that file overlap and label persistence bias can inflate within-project SDP performance at file granularity. JIT-SDP instead targets the individual commits, so risky changes can be reviewed as soon as they are submitted. The idea goes back to the change-level risk models of Mockus and Weiss (2000), and its modern formulation was established by the large-scale empirical study of Kamei

et al. (2013). That study introduced a set of change-level metrics that is now standard, covering the size, diffusion, history, and developer experience of a change, together with effort-aware evaluation that ranks changes by defect likelihood per unit of inspection effort. Training labels are commonly derived using the SZZ algorithm, which traces bug-fixing commits back to the changes that likely introduced the defect (Śliwerski et al., 2005). Early work formulated the problem as a binary classification task, predicting whether each change is clean or buggy (Kim et al., 2008). Later studies examined how such models generalize across projects (Fukushima et al., 2014; Kamei et al., 2016) and how they degrade over time, with McIntosh and Kamei (2018) showing that fix-inducing changes are a moving target.

A first wave of learning-based approaches moved beyond hand-crafted metrics by learning richer representations from traditional change features. Yang et al. (2015b), for example, used a deep belief network to transform conventional metrics into higher-level features. Later work shifted toward end-to-end representation learning. DeepJIT (Hoang et al., 2019) learns from commit messages and code changes, while CC2Vec (Hoang et al., 2020) learns representations of code changes using their associated log messages. Other studies have targeted finer-grained prediction, identifying defect-prone files or lines within a commit (Pascarella et al., 2019; Pornprasit and Tantithamthavorn, 2021), while complementary work has focused on explaining predictions to developers (Pornprasit et al., 2021).

More recent approaches have incorporated pre-trained code models. JIT-Fine combines semantic representations from CodeBERT with expert-designed features (Ni et al., 2022), bi-modal pre-training further improves the representation of code changes (Jiang et al., 2025), and parameter-efficient tuning reduces the cost of adapting such encoders (Abu Talib et al., 2024). At the same time, several studies have questioned whether increasingly complex models are always necessary. Zeng et al. (2021) show that a simple model based on a single churn feature can match complex approaches, while other work finds benefits in combining expert knowledge with learned semantic representations (Zhou et al., 2025; Chen et al., 2023). IRJIT similarly demonstrates that a lightweight information-retrieval approach can remain competitive while offering much lower prediction cost (Sahar et al., 2024).

Two practical issues have become increasingly important in JIT-SDP. One is the online nature of the task. Commits arrive as a stream, labels become available only after a verification latency, and the class distribution drifts. Cabral and Minku (2023) study reliable online JIT-SDP under these conditions, while Tabassum et al. (2023) extend the setting to cross-project online learning. The other issue is how a code change is represented. Flat metrics and token sequences largely ignore the relational structure surrounding a change. Bryan and Moriano (2023) address this limitation by constructing contribution graphs over developers and files. The survey by Zhao et al. (2023) likewise identifies richer structural and semantic modeling as an important direction for future work, while methodological studies emphasize the need for rigorous model validation (Tantithamthavorn et al., 2017).

Our work builds on this perspective but shifts the focus from developer–file relationships to the changed code itself and its broader project context, represented as an evolving knowledge graph.

2.2. *Software Defect Prediction and Code Representation*

Defect prediction has long been studied at the file and module level. Early approaches relied on static code properties, such as size and complexity metrics (Menzies et al., 2007), while a parallel line of work showed that change and process information, including code churn and properties of the change history, can be even more predictive (Nagappan and Ball, 2005; Moser et al., 2008; Hassan, 2009). Subsequent empirical studies and benchmarks compared classifiers and datasets under common evaluation settings (Lessmann et al., 2008; Hall et al., 2012; D'Ambros et al., 2012). Another substantial body of work examined cross-project defect prediction, where models are transferred across projects when project-specific training data are limited (Zimmermann et al., 2009; Nam et al., 2013). Together, these studies established many of the features, datasets, and evaluation practices that later defect-prediction research builds upon.

A second line of work learns representations from code without relying on hand-crafted metrics. This direction is motivated by the observation that source code exhibits regular and predictable patterns similar to natural language (Hindle et al., 2012), making distributed representation learning a natural fit (Mikolov et al., 2013). Wang et al. (2016) learn semantic features from token sequences derived from abstract syntax trees (ASTs) using a deep belief network, while convolutional and tree-based models capture syntactic structure (Mou et al., 2016; Li et al., 2017; Tai et al., 2015). Other approaches represent programs through AST fragments, including path-based models such as

code2vec (Alon et al., 2019b) and code2seq (Alon et al., 2019a), and statement-level encoders such as ASTNN (Zhang et al., 2019a). More recently, self-supervised pre-training has become a common foundation for code representation learning. Representative models include InferCode (Bui et al., 2021), contextual code embeddings learned with large Transformers (Kanade et al., 2020), CodeBERT (Feng et al., 2020), GraphCodeBERT (Guo et al., 2021), and CodeT5 (Wang et al., 2021). Related work also augments sequence models with global relational information to better capture dependencies that are difficult to express through token order alone (Hellendoorn et al., 2020).

Since trees and token sequences capture only part of a program's structure, a growing body of work represents code as graphs and learns over them with graph neural networks (Scarselli et al., 2009; Wu et al., 2021). Allamanis et al. (2018) augment ASTs with data-flow and apply gated graph neural networks (Li et al., 2016), while Devign (Zhou et al., 2019) combines AST, control-flow, and data-flow information in a unified graph for vulnerability detection. Graph-based representations have also been adopted in defect prediction. Zhou et al. (2022) combine ASTs with class-dependency networks, Liu et al. (2023a) enrich code representations with external knowledge, and Šikić et al. (2022) apply graph neural networks over ASTs for module-level prediction.

Related work further shows the value of augmenting syntax trees with flow information for code analysis tasks (Wang et al., 2020). Recent surveys reflect this broader shift toward deep and structurally informed representations in defect prediction (Zain et al., 2023). These approaches demonstrate the value of modeling program structure, but they largely remain confined to individual files or modules and do not simultaneously capture project-wide context and satisfy the online constraints of JIT-SDP.

2.3. Knowledge Graphs and Their Applications

Knowledge graphs (KGs) represent information through entities and typed relations, providing a foundation for reasoning, retrieval, and learning (Hogan et al., 2021; Ji et al., 2022; Nickel et al., 2016). Much of the literature focuses on learning continuous representations of these entities and relations so that symbolic knowledge can be incorporated into machine learning models (Ji et al., 2022; Wang et al., 2017). Early approaches include tensor-factorization methods such as RESCAL (Nickel et al., 2011) and translational models such as TransE (Bordes et al., 2013), TransH (Wang et al., 2014), and TransR (Lin et al., 2015), which represent relations through transformations in the embedding space. Later models improve expressiveness through bilinear or complex-valued scoring functions, including DistMult (Yang et al., 2015a), ComplEx (Trouillon et al., 2016), and RotatE (Sun et al., 2019). Neural approaches extend this line further, with models such as ConvE (Dettmers et al., 2018), relational graph convolutional networks (Schlichtkrull et al., 2018), and composition-based message-passing methods (Vashishth et al., 2020) learning over multi-relational graph structure.

Knowledge graphs have been applied across a wide range of domains. Large general-purpose resources such as YAGO, Freebase, and Wikidata demonstrated that relational knowledge can be organized and queried at web scale (Suchanek et al., 2007; Bollacker et al., 2008; Vrandečić and Krötzsch, 2014). In recommender systems, knowledge graphs help alleviate data sparsity and support more interpretable recommendations, as illustrated by KGAT (Wang et al., 2019), RippleNet (Wang et al., 2018), and the broader literature surveyed by Guo et al. (2022). They have also been used to integrate biomedical evidence for drug discovery (MacLean, 2021), consolidate cyber-threat intelligence (Zhao et al., 2024), and incorporate structured knowledge into language models (Zhang et al., 2019b).

Dynamic knowledge graphs further extend this framework by modeling how entities and relations evolve over time (Zhang et al., 2024; Cai et al., 2024; Trivedi et al., 2017; Goel et al., 2020; Jin et al., 2020; Lacroix et al., 2020). Within software engineering, knowledge graphs have mainly been used to organize and connect software artifacts such as APIs and libraries (Wang et al., 2023; Liu et al., 2023b). For example, Liu et al. (2023b) embed an API knowledge graph to recommend analogous APIs. In contrast, knowledge graphs remain largely unexplored across software defect prediction. To the best of our knowledge, no prior work has used knowledge graphs or comparable relational representations to incorporate project-wide context into JIT-SDP.

3. Methodology

3.1. Motivation

JIT-SDP must quickly provide feedback as a change is submitted (Kamei et al., 2013). Existing models therefore rely largely on features extracted from the current commit, such as code diffs and churn metrics (Kamei et al., 2013; Hoang et al., 2019; Nagappan

and Ball, 2005), but these features omit broader repository context, including information around changed lines, developer experience, and developer–file relationships (Kondo et al., 2020; Cho et al., 2022; Bryan and Moriano, 2023). Maintaining and efficiently integrating such context is challenging in a just-in-time setting (Kondo et al., 2020; Bryan and Moriano, 2023). KG-Commit instead maintains it incrementally in Neo4j. Each commit updates only the affected graph neighborhood, so the accumulated project context is available at prediction time through bounded Cypher queries.

3.2. Problem Formulation

Let a software project P be represented as a chronologically ordered sequence of commits $C = \{c^{(1)}, c^{(2)}, \ldots, c^{(n)}\}$. Each commit $c^{(i)} \in C$ represents an evolutionary step that alters the state of the project from $s^{(i-1)}$ to $s^{(i)}$. Each commit $c^{(i)}$ targets a set of pre-existing files $F^{(i)}_{\text{prev}} = \{f_1, f_2, \ldots, f_m\}$ and produces a set of modified or newly created files $F^{(i)}_{\text{new}} = \{f'_1, f'_2, \ldots, f'_p\}$. Therefore, a commit may add, remove, modify, or rename/move one or more files in the project.

3.2.1. Defect Modeling

A commit $c^{(i)}$ is defined as bug-inducing if and only if it introduces a defect into the codebase that requires a subsequent fix. Formally, we define the ground-truth binary label $y^{(i)} \in \{0, 1\}$ for each commit with index $i \geq 1$ as

$$y^{(i)} = \begin{cases} 1 & \text{if } \exists f \in F^{(i)}_{\text{new}} \text{ such that } f \text{ is defective} \\ 0 & \text{otherwise} \end{cases} \tag{1}$$

In our experiments, we use the labels provided by the ApacheJIT dataset (Keshavarz and Nagappan, 2022), where bug-inducing commits are identified using an SZZ-style algorithm.

3.2.2. Operational Constraints

To simulate real-world deployment settings, the online formulation introduces two constraints: a warm-up period t and a gap g (Lee et al., 2024; Song et al., 2023). The warm-up period requires t commits to be processed before evaluation begins, restricting the target commit $c^{(j)}$ to indices where $j > t$. The gap g accounts for the operational delay in defect identification (e.g., via the SZZ algorithm), meaning that when commit $c^{(j)}$ arrives, historical ground-truth labels are only resolved and available up to commit $c^{(j-g-1)}$.

3.2.3. Online Predictive Objective

Given a target commit $c^{(j)}$, where $j > t$, the objective is to estimate the conditional probability $\hat{y}^{(j)}$ that the commit is bug-inducing based on the current project state $s^{(j-1)}$:

$$\hat{y}^{(j)} = \hat{\mathbb{P}}\left(y^{(j)} = 1 \,\middle|\, c^{(j)}, s^{(j-1)}\right) \tag{2}$$

3.2.4. Knowledge Graph State Representation and Evolution

To avoid recomputing deep repository histories on demand, the abstract project state and its evolutionary history are captured by an incrementally updated knowledge graph $\mathcal{K}^{(j)}$. Upon the arrival of a target commit $c^{(j)}$, its corresponding entities and relations are immediately updated and inserted into the graph before classification occurs. This state evolution follows a recurrence relation defined by a state transition function Φ:

$$\mathcal{K}^{(j)} = \Phi\left(\mathcal{K}^{(j-1)}, c^{(j)}, y^{(j-g-1)}\right) \tag{3}$$

where $c^{(j)}$ provides the immediate modifications for the incoming commit, and $y^{(j-g-1)}$ injects the historical ground-truth label newly exposed by the expiration of the gap window. By unrolling this recurrence, $\mathcal{K}^{(j)}$ preserves the complete history of previous project states and commits:

$$\mathcal{K}^{(j)} = \text{Encode}\left(\{s^{(i)}\}_{i=1}^{j},\ \{c^{(i)}\}_{i=1}^{j},\ \{y^{(i)}\}_{i=1}^{j-g-1}\right), \tag{4}$$

in the sense that all this information can later be accessed or reconstructed. In our case, this is made possible by using appropriate Cypher queries against the graph database.

Because $\mathcal{K}^{(j)}$ embeds this entire history alongside the unlabeled properties of the recent commits, the predictive objective is resolved by conditioning on the new graph state:

$$\hat{y}^{(j)} = \hat{\mathbb{P}}\left(y^{(j)} = 1 \,\middle|\, \mathcal{K}^{(j)}\right) \tag{5}$$

3.3. KG-Commit

KG-Commit models the evolving repository as a three-layer knowledge graph whose entity and relation schema is summarized in Table 1, while the overall online workflow is illustrated in Figure 2. The Core layer captures repository-level development context, the AST layer represents within-file program structure through an AST and updates it incrementally using delta extraction, and the Commit Semantic-Text Graph

(CSTG) adds information from commit messages and diff text through graph-of-words statistics, term associations, and propagated defect risks. Commits are processed chronologically and inserted into Neo4j. The graph is updated through Cypher operations, and only information available at that point in time is queried for prediction. The resulting graph is then used by the inference channels through a compact projection, with selected context taken from the full graph, and their outputs are combined to estimate the defect risk of the current commit.

Table 1: Typed schema of KG-Commit.

Relation	Source → Target	Description
Core layer *Entities:* `Commit`, `Developer`, `File`, `Issue`		
`AUTHORED_BY`	`Commit` → `Developer`	Records commit authorship.
`PARENT_OF`	`Commit` → `Commit`	Represents repository history.
`FIXES_ISSUE`	`Commit` → `Issue`	Links a commit to an issue.
`ADDED/MODIFIED/DELETED`	`Commit` → `File`	Records file-level changes.
`RENAMED_FROM/RENAMED_TO`	`Commit` → `File`	Records old/new paths of a rename.
`IMPORTS`	`File` → `File`	Plain import.
AST layer *Entities:* `ASTNode`, `Package`		
`HAS_AST`	`File` → `ASTNode`	Attaches a file to its AST root.
`AST_CHILD`	`ASTNode` → `ASTNode`	Ordered AST parent–child relation.
`ADDS/REMOVES/UPDATES/MOVES`	`Commit` → `ASTNode`	Records the structural delta.
`RESOLVES_TO`	`ASTNode` → `File`	Resolves a static-member import to its owning type file.
`RESOLVES_TO_PACKAGE`	`ASTNode` → `Package`	Resolves a wildcard import to its package.
`CONTAINS`	`Package` → `File`	Records files belonging to a package.
CSTG layer *Entities:* `Term`, `Intent`		
`MENTIONS`	`Commit` → `Term`	Records terms occurring in a change.
`COOCCURS`	`Term` → `Term`	NPMI-based term association.
`HAS_INTENT`	`Commit` → `Intent`	Assigns the commit's intent.
`GROUNDS_IN`	`Term` → `ASTNode`	Grounds code terms in matching AST leaves.

3.3.1. Cypher Queries

KG-Commit is stored in Neo4j and accessed through Cypher, its declarative graph query language (Francis et al., 2018). Cypher specifies graph patterns through labeled nodes and typed relationships, such as `(c:Commit)` and `-[:MODIFIED]->`. During construction, `MERGE` avoids duplicate nodes and relationships by creating them only when they are not already present, while `UNWIND` enables multiple relationships to be processed in a single database request. Figure 3 shows a Core-layer query that upserts a `Commit` node and batch-creates its `MODIFIED` relationships to `File` nodes. At prediction time, `MATCH` retrieves the local neighborhood required by the inference methods.

3.3.2. Layer 1: Core Components

The Core layer captures the repository's high-level entities and their basic relations (see Figure 4). Each commit becomes a `Commit` node, and its bug-inducing label is attached when it becomes available; it is linked to its author (`AUTHORED_BY`), its children (`PARENT_OF`), the issues referenced in its message (`FIXES_ISSUE`), and the files it changes, with the edge type recording the kind of change (`ADDED`, `MODIFIED`, `DELETED`, `RENAMED_FROM`, or `RENAMED_TO`). The layer also captures cross-file dependencies through `IMPORTS`. These edges are maintained over time so that both current and historical dependencies remain represented.

3.3.3. Layer 2: Within-File AST Subgraph

The AST layer captures the syntactic structure of Java files using a deterministic AST representation. Each file is parsed with `javalang`, and its parse tree is traversed in pre-order to construct the corresponding subgraph. For a file with repository-relative path *rel*, the i-th visited node is assigned the identifier $rel\texttt{::A}[i]$. Each `ASTNode` records its `javalang` type, syntactic category, and a compact value when applicable, such as an identifier, literal, or operator; non-blank string children are represented as `Identifier` leaves. To ensure that the same source produces the same graph across runs, ordered child containers keep their original order, whereas unordered containers are canonically sorted. The resulting AST is attached to its `File` through `HAS_AST`, while `AST_CHILD` relations encode the parent–child relations and child positions.

AST matching and delta extraction. For a modified file, let A^b and A^a be the stored and newly parsed ASTs. The matcher constructs a partial injective correspondence $\mu : V(A^b) \rightharpoonup V(A^a)$ in three stages. First, each node is assigned a bottom-up fingerprint: Let $u_1, \ldots, u_k$ be the ordered children of v, and define $h(v) = H(\ell(v)\|h(u_1)\|\cdots\|h(u_k))$ where $\ell(v) = \texttt{ast_type}(v)\|\texttt{value}(v)$. Here, $\|$ denotes an unambiguous concatenation and H is the MD5 message-digest algorithm (Rivest, 1992). This bottom-up construction is

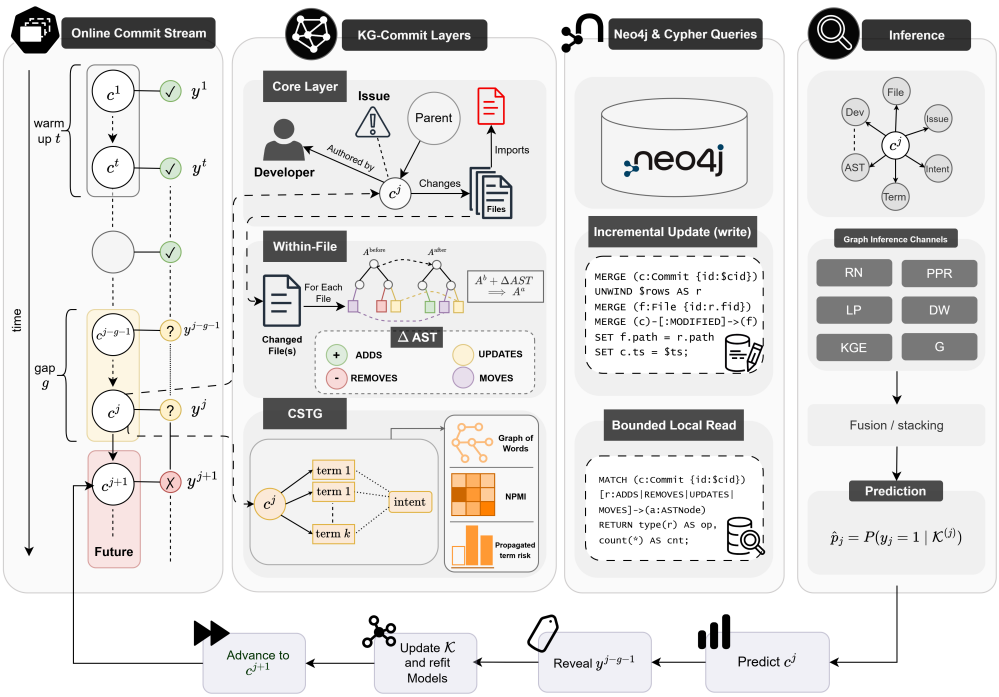

Figure 2: Overview of KG-Commit's online workflow.

```
// (1) upsert an entity node by primary key
MERGE (e:Commit {id: $pk_value})
  ON CREATE SET e += $props
  ON MATCH  SET e += $props

// (2) batch-create the process edges from one source
      node
MATCH (src:Commit {id: $src_id})
UNWIND $targets AS t
  MERGE (tgt:File {id: t.target_id})
  MERGE (src)-[r:MODIFIED]->(tgt)
    ON CREATE SET r += t.props
```

Figure 3: Core-layer Cypher query: (1) upserts a `Commit` node by its identifier, and (2) batch-creates `MODIFIED` relationships to the corresponding `File` nodes.

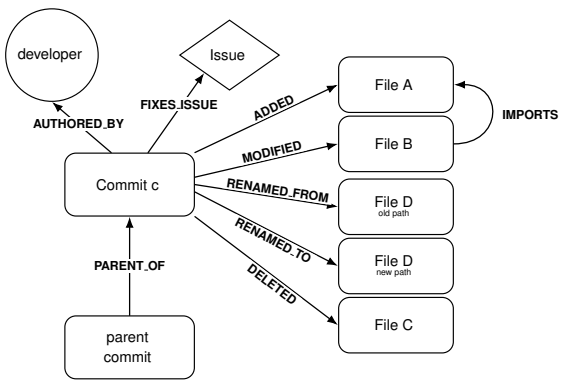

Figure 4: Illustration of the Core layer.

commonly known as subtree hashing or syntax-tree fingerprinting (Chilowicz et al., 2009). Equal fingerprints identify candidate identical subtrees. Larger candidate subtrees are processed first, with source position used to break ties, following the general strategy of prioritizing large isomorphic subtrees in AST differencing (Falleri et al., 2014). Second, matches are propagated to unmatched parents of the same AST type until a fixpoint is reached. Third, remaining nodes are matched by (`ast_type`, `line`, `column`) whenever this tuple is unique. The unmatched and changed nodes define the delta:

$$R = V(A^b) \setminus \mathrm{dom}(\mu), \tag{6}$$

$$A = V(A^a) \setminus \mathrm{ran}(\mu), \tag{7}$$

$$U = \left\{ (b,a) \in \mu \;\middle|\; \begin{array}{l} \texttt{ast_type}(b) \neq \texttt{ast_type}(a) \\ \vee\ \texttt{value}(b) \neq \texttt{value}(a) \end{array} \right\}, \tag{8}$$

$$M = \left\{ (b,a) \in \mu \;\middle|\; \begin{array}{l} \mathrm{par}(b) \in \mathrm{dom}(\mu) \\ \wedge\ \mu(\mathrm{par}(b)) \neq \mathrm{par}(a) \end{array} \right\}. \tag{9}$$

Here, R, A, U, and M denote `REMOVES`, `ADDS`, `UPDATES`, and `MOVES` respectively. Figure 5 illustrates the resulting correspondence and edit classes.

Online delta maintenance. Commits are processed in chronological order while the system preserves, for each

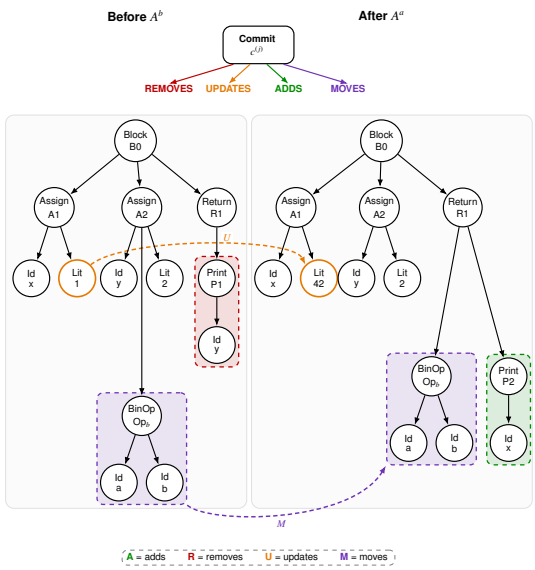

Figure 5: Simplified illustration of AST deltas between the before tree A^b and the after tree A^a.

tracked file, its current AST and the mapping from parse identifiers to persistent graph identifiers. Added files are materialized once, files first encountered as modifications are initialized from their parent revision, and deleted files have their live nodes marked inactive. During a modification, matched nodes keep their identifiers, inserted nodes receive new identifiers, and removed nodes remain queryable through `alive=` FALSE. The live `AST_CHILD` relations are updated in place, while the commit stores only the resulting `ADDS`, `REMOVES`, `UPDATES`, and `MOVES` relations. Thus, storage and update costs follow the amount of syntactic change.

Alternative within-file representations. Besides AST, we evaluate control-flow graph (CFG), data-flow graph (DFG), and program dependence graph (PDG) as alternative within-file representations. Each representation is mapped to the same `ADDS`, `REMOVES`, `UPDATES`, and `MOVES` delta vocabulary used for AST, where CFG, DFG, and PDG use a graph-specific ordinal matcher rather than the tree-specific AST matcher (see Appendix A for details).

3.3.4. Layer 3: Commit Semantic-Text Graph (CSTG)

The third layer represents the semantics of a change using its commit message and diff text. For each commit c, we concatenate the message with lexical tokens from changed lines to form x_c. The text is tokenized and lower-cased, camel-case identifiers are split, and defect-relevant identifiers such as `*Exception` and `*Error` are preserved. Terms are assigned types in {code, bug, action, error, natural-language}. The extraction rules for these types are summarized in Table 2. Each commit yields a graph-of-words whose terms are linked to the commit through weighted `MENTIONS` relations. Across previously observed commits, associated terms are connected through `COOCCURS`, and each term receives a defect-risk estimate obtained from past observations and propagated through this term-association graph. The resulting CSTG schema is illustrated in Figure 6.

Table 2: Term types used by CSTG and their extraction rules.

Type	Extraction rule
error	Identifiers denoting exception or error types, including identifiers ending in `Exception` or `Error`.
code	Program identifiers recognized from camel-case, snake-case, or dotted forms.
bug	Terms belonging to a fixed defect vocabulary, including concepts such as `npe`, `leak`, `race`, `deadlock`, and `regression`.
action	Terms belonging to a fixed change-action vocabulary, such as `add`, `fix`, `refactor`, and `revert`.
natural-language	Remaining lexical terms, including subwords obtained by splitting compound program identifiers.

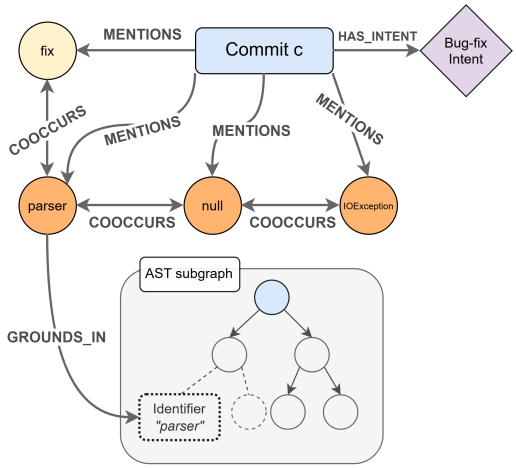

Figure 6: CSTG schema for a commit. Darker term nodes indicate higher propagated defect risk.

Commits are also linked to `Intent` nodes through `HAS_INTENT`. Each commit receives exactly one intent from {FIX, FEAT, REFACTOR, TEST, DOCS, PERF, REVERT, OTHER}. Intent is assigned by a deterministic keyword rule over the lower-cased commit message; occurrences of the keywords associated with each class are counted, the highest-scoring class is selected, and OTHER is returned when no keyword matches. Repeated occurrences contribute repeatedly to the class score. The complete taxonomy is given in Table 3. The `GROUNDS_IN` relation provides the bridge from CSTG to the AST layer (Section 3.3.3). It is created only for *code* `Term` nodes and connects them to live AST leaves whose stored value exactly equals the term text. Deleted AST nodes are excluded, and the number of matching leaves is capped for highly common identifiers.

Table 3: Intent taxonomy and keyword rules used by CSTG. Truncated stems such as `optimi` and `deprecat` intentionally match multiple inflected forms.

Intent	Keywords
FIX	`fix`, `bug`, `issue`, `error`, `fault`, `defect`, `npe`, `crash`, `fail`, `correct`, `resolve`, `patch`, `wrong`, `broken`
FEAT	`add`, `feature`, `implement`, `introduce`, `support`, `new`, `allow`, `enable`, `provide`
REFACTOR	`refactor`, `cleanup`, `clean up`, `simplify`, `rename`, `reorganize`, `restructure`, `tidy`, `inline`, `extract`, `deprecat`
TEST	`test`, `junit`, `assert`, `testcase`, `coverage`, `spec`
DOCS	`doc`, `documentation`, `javadoc`, `readme`, `comment`, `license`
PERF	`perf`, `performance`, `optimi`, `speed`, `faster`, `cache`, `latency`
REVERT	`revert`, `rollback`, `roll back`, `undo`, `back out`
OTHER	No keyword from the preceding classes occurs.

For each commit c, the distinct normalized terms V_c form a weighted graph-of-words in which terms co-occurring within a window of w tokens are connected (Rousseau and Vazirgiannis, 2013), preserving local dependencies that a bag-of-words model discards (Rousseau and Vazirgiannis, 2015). Each term receives a weighted TextRank score $\mathrm{TR}_c(t)$ with damping factor d (Mihalcea and Tarau, 2004), and its `MENTIONS` weight is $m_c(t) = \mathrm{TR}_c(t)\log((|C_{\mathrm{tr}}|+1)/(\mathrm{df}(t)+1))$, combining within-commit centrality with corpus-level rarity as a TextRank-based variant of graph term-weight IDF (Rousseau and Vazirgiannis, 2013).

Across training commits, term associations are measured by NPMI (Church and Hanks, 1990; Bouma, 2009); a `COOCCURS` edge is kept only when its support is at least $n_{\min}$ and its NPMI is at least τ_{T}. Each term is initialized with smoothed defect risk $r^{(0)}(t) = (\mathrm{bugdf}(t) + \lambda\bar{y})/(\mathrm{df}(t) + \lambda)$ and propagated over the row-normalized term graph as $r^{\star} = (1 - \alpha_{\mathrm{T}})r^{(0)} + \alpha_{\mathrm{T}}P_{\mathrm{T}}r^{\star}$, imposing smoothness over associated terms (Belkin et al., 2006). CSTG finally summarizes this information through the weighted textual-risk prior $\rho(c) = \sum_t m_c(t)r^{\star}(t)/\sum_t m_c(t)$ and type-specific semantic masses $M_{\kappa}(c) = \sum_{\mathrm{type}(t)=\kappa} m_c(t)$ for the five term types defined above. An example of the resulting global term graph is shown in Figure 7.

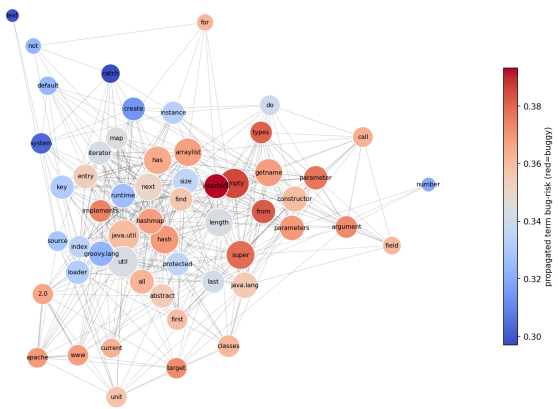

Figure 7: Example of global CSTG term graph. Edges denote retained positive NPMI associations, and node color indicates propagated term risk $r^{\star}(t)$.

3.3.5. *Inference over KG-Commit*

We use five graph-based inference channels: Relational Neighbor (RN) (Macskassy and Provost, 2003), Personalized PageRank (PPR) (Haveliwala, 2002), clamped Label Propagation (LP) (Zhu et al., 2003), DeepWalk matrix factorization (DW) (Perozzi et al., 2014), and DistMult knowledge-graph embedding (KGE) (Yang et al., 2015a). A sixth, feature-based G channel uses the semantic statistics derived from components in Section 3.3.4 (see Appendix D for full construction details).

3.3.6. Projection for Lightweight Graph Inference

The five graph-based inference methods operate on a compact projection of KG-Commit. At commit j, this projection summarizes the neighborhood of each commit in the full graph as a weighted bipartite graph $\mathcal{P}^{(j)}$. RN, PPR, LP, DW, and KGE operate on this smaller graph, keeping graph inference practical on CPU. The construction of the projection and the corresponding inference procedures are described in Appendix C.

The projection does not include every relation in the full graph. For example, cross-file `IMPORTS` relations remain in $\mathcal{K}^{(j)}$ and are not part of $\mathcal{P}^{(j)}$. We therefore also derive a small traversal/global-context (TGC) vector from the full graph. For a commit c, we denote this vector by

$$\mathbf{T}(c) = \left[\mathbf{T}_0(c), \mathbf{T}_{1,\text{dep}}(c), \mathbf{T}_{1,\text{dry}}(c), \mathbf{T}_P(c), \mathbf{M}_1(c)\right].$$

The grouped vector covers the files changed by the commit ($\mathbf{T}_0(c)$), their untouched importers and importees, split by direction ($\mathbf{T}_{1,\text{dep}}(c)$ and $\mathbf{T}_{1,\text{dry}}(c)$), files in the same package ($\mathbf{T}_P(c)$), and their architectural position in the dependency graph ($\mathbf{M}_1(c)$), summarized using PageRank and k-core (Brin and Page, 1998; Batagelj and Zaversnik, 2003). The extracted values are cached and used together with the projection-based inference scores. The individual TGC features and their computation are described in Appendix E.

Score fusion. We use logistic-regression stacking (Wolpert, 1992) to combine the different inference outputs. Let $\mathrm{F} \subseteq \{\mathrm{RN}, \mathrm{PPR}, \mathrm{LP}, \mathrm{DW}, \mathrm{KGE}\}$ denote a selected set of graph-based channels, with $s_m(c)$ denoting the score of channel m. We use F for their stacked combination, G for the CSTG channel, F + G for their joint model, and F + G + T when the TGC features $\mathbf{T}(c)$ are also included. The full model is

$$\widehat{y}(c) = \sigma\left(\theta_0 + \sum_{m \in F} \theta_m s_m(c) + \theta_G G(c) + \boldsymbol{\theta}_T^\top \mathbf{T}(c)\right),$$

where θ_0 is the intercept, θ_m and θ_G are the coefficients of the graph and CSTG scores, and $\boldsymbol{\theta}_T$ contains the coefficients of the TGC features. Removing the corresponding terms gives the F and $F + G$ variants. For deployment, a fixed overall subset $F_{\text{ov}} \subseteq F$ may be used across projects (see Section 4.4).

4. Experimental Design

The objective of this study is to determine whether KG-Commit can make rich, project-wide context practically usable for online JIT-SDP. To achieve this objective, we formulate four main research questions as follows:

4.1. Research Questions

- **RQ1.** *What is the predictive performance of KG-Commit in Just-in-Time Software Defect Prediction?*
- **RQ2.** *How well does KG-Commit maintain computational efficiency and scalability across the real-time evolution of different software projects?*
- **RQ3.** *How do architectural choices regarding within-file subgraph representations and distinct KG-Commit layers affect the predictive performance?*
- **RQ4.** *How does KG-Commit's predictive performance change across different inference channels?*

4.2. Dataset

We perform the evaluation on 11 software projects from ApacheJIT (Keshavarz and Nagappan, 2022). The selected projects, shown in Table 4, contain 78,206 evaluated commits, of which 22,740 are bug-inducing and 55,466 are clean, corresponding to an overall bug-inducing rate of approximately 29.1%. Labels are produced using the SZZ algorithm (Śliwerski et al., 2005) and refined by linking fixes to issue reports and filtering trivial edits with GumTree over abstract syntax trees, following established filtering procedures (McIntosh and Kamei, 2018). Each commit is described by fourteen fields: a commit identifier, the binary bug-inducing label, and twelve change metrics that follow the definitions of Kamei et al. (2013). Because these metrics are highly right-skewed, we apply a logarithmic transform.

4.3. Baselines

Logistic Regression (LR). It is the classical change-metric baseline used in JIT-SDP (Kamei et al., 2013). It operates on the twelve ApacheJIT change metrics after the transformations described in Section 4.2 and uses ℓ_2-regularized logistic regression with balanced class weights.

Table 4: ApacheJIT projects used in the evaluation (Keshavarz and Nagappan, 2022). Percentages give the ratio of bug-inducing commits to total evaluated commits.

Project	Bug-inducing	Clean	Total
ActiveMQ	1,404 (23%)	4,722	6,126
Camel	3,078 (14%)	19,617	22,695
Cassandra	3,117 (38%)	5,042	8,159
Flink	2,811 (25%)	8,648	11,459
Groovy	1,614 (20%)	6,445	8,059
HBase	3,782 (43%)	4,945	8,727
Hive	4,223 (62%)	2,619	6,842
Kafka	1,115 (47%)	1,269	2,384
Spark	632 (43%)	833	1,465
Zeppelin	622 (43%)	829	1,451
Zookeeper	342 (41%)	497	839
Total	**22,740 (29.1%)**	**55,466**	**78,206**

Histogram Gradient Boosting (HGB). It uses the same twelve change metrics but replaces the linear decision function with a histogram-based gradient-boosting classifier. It provides a non-linear change-metric baseline while keeping the input information identical to LR. Class weighting is used to account for label imbalance.

Random Forest (RF). RF uses the same twelve ApacheJIT change metrics and the same feature-extraction pipeline as LR and HGB, differing only in the classifier.

LApredict (Zeng et al., 2021). This baseline deliberately uses only the number of added lines. We implement it using the same class-weighted logistic-regression family as LR.

DeepJIT (Hoang et al., 2019). Our implementation follows the official DeepJIT architecture, with separate convolutional encoders for the commit message and changed code, a hierarchical convolution over changed code lines, concatenation of the message and code representations, a 512-unit fully connected layer, and a sigmoid output. The implementation is adapted to our online evaluation setting.

JITLine (Pornprasit and Tantithamthavorn, 2021). This method combines the twelve expert change metrics with token information extracted from the code diff and trains a random-forest classifier on the resulting representation. The implementation is adapted to our online evaluation setting.

4.4. Experimental Protocol

Evaluation follows an online protocol. For each incoming commit, a prediction is produced using only the information at that point in the stream. The labels enter the historical state only after they become available under the gap parameter g introduced in Section 3.2.2. Let K denote the warm-up fraction and $t = \lfloor KN \rfloor$ for a project with N commits. Commits before t initialize the graph. The refit window M determines how often model components are refitted, while commits are still processed one by one. We use a shared setting of $K = 0.05$ and $g = 50$ for KG-Commit and baselines, and $M = 200$ for all learnable models that need a refit. Threshold-dependent metrics use an online operating point. The threshold is initialized at 0.5 and, after the first 300 predictions, is re-estimated every 150 commits to maximize Macro-F1 on past commits.

Throughout Section 5, F_{ov} denotes the fixed graph fusion RN, PPR $\subseteq F$ (Section 3.3.5); the rationale for this choice is examined in Section 5.4. The primary KG-Commit configuration augments F_{ov} with the semantic CSTG channel G and the traversal/global-context feature block T, forming F_{ov}+G+T (Section 3.3.6). Unlike the graph channels, G requires sufficient history to construct a vocabulary and is therefore unreliable during cold start. The S@200 policy addresses this problem by using F_{ov} alone for the first 200 evaluated commits after warm-up and then switching once to F_{ov}+G for the remainder of the stream, as discussed further in Section 6.3. The addition of T does not change the definition of this switch. S@200 continues to denote the one-time introduction of the history-dependent configuration and is distinct from the periodic refit interval $M = 200$. Unless an experiment explicitly performs a controlled ablation or sensitivity analysis, the reported KG-Commit result corresponds to F_{ov}+G+T. For compactness, tables and figures may denote this configuration as F+G+T, with $F = F_{\text{ov}}$.

Reproducibility of Results Across Different Runs. We assessed seed sensitivity across five runs. The F_{ov}+G backbone reproduces to numerical precision, and the added TGC extraction and `liblinear` stacking head are deterministic for a fixed commit stream, so T does not introduce an additional source of random variation. Graph-only fusions containing learned channels show greater run-to-run variation, as examined in Section 5.4. LR and LApredict are deterministic, HGB shows negligible variation (3.9×10^{-4} in Macro-F1), and JITLine-online is evaluated with a fixed random state. Only RF and DeepJIT exhibit noticeable seed sensitivity, with mean Macro-F1 standard deviations of

0.0097 and 0.0102, respectively. Given this limited variation, Section 5 reports aggregate performance only.

4.5. Experimental Settings

Table 5 summarizes the model configurations and hyperparameters used throughout the experiments, while Table 6 reports the corresponding execution environments and software stacks. The reported settings are fixed across projects, and parameters not listed in the tables keep their implementation defaults. KG-Commit and all non-neural baselines are executed in the same CPU environment. DeepJIT (Hoang et al., 2019), which requires repeated training of convolutional neural components, is implemented and executed separately in a Kaggle notebook using a single NVIDIA Tesla T4 GPU. Because DeepJIT is executed on different hardware, its runtime is reported for completeness only and should be excluded from hardware-matched runtime comparisons.

4.6. Evaluation Metrics

Given the class imbalance of bug-inducing commits, we primarily report Macro-F1, AUC, and G-Mean $= \sqrt{\text{TPR} \cdot \text{TNR}}$ as class-balanced measures. We also use two effort-aware metrics with inspection effort defined as `la` + `ld`, including the normalized P_{opt}, which measures how closely the effort-ranked inspection order approaches the optimal buggy-first, least-effort-first ranking, and ACC@20%LOC (Kamei et al., 2013), which measures the proportion of bug-inducing commits found within the top 20% of cumulative changed lines.

Average rows in Section 5 report an unweighted macro-average over projects and a micro-average over their pooled predictions. For runtime and lifecycle measurements in Section 5.2, we report the mean, standard deviation (SD), median, and selected percentiles where appropriate. P05, P50, and P95 denote the 5th, 50th, and 95th percentiles, respectively, representing the lower tail, median, and upper tail of the observed distribution.

5. Experimental Results

5.1. RQ1: Predictive Performance against Baselines

KG-Commit achieves the highest aggregate Macro-F1, G-Mean, and AUC among the evaluated methods (Table 7), with their project-level distributions shown in Figure 8. It improves Macro-F1 over RF (0.649 → 0.704), LApredict (0.637 → 0.704), HGB (0.636 → 0.704), DeepJIT (0.618 → 0.704), LR (0.579 → 0.704), and JITLine-online (0.674 → 0.704). The

Table 5: Model hyperparameters and configurations used for KG-Commit and the evaluated baselines.

Component / Parameter	Value
KG-Commit graph inference	
Relational Neighbor (RN)	
Neighborhood depth	1 hop
Learned embedding	None
Personalized PageRank (PPR)	
Restart probability α	0.15
Power iterations	40
Label Propagation (LP)	
Propagation iterations	3
DeepWalk (DW)	
Matrix representation	PPMI
Factorization	Truncated SVD
Embedding dimension	64
DistMult (KGE)	
Embedding dimension	32
Optimizer	SGD
Learning rate η	0.05
Epochs per refit	3
Negative samples per positive	3
Triple-update chunk size	2,048
Classifier heads	
Classifier	Logistic Regression
Solver	`lbfgs`
Class weighting	`balanced`
Maximum iterations	1000
CSTG semantic channel	
TextRank damping factor	0.85
TextRank iterations	30
Minimum term co-occurrence	2
Risk-prior smoothing constant	5
Hashed-text dimension	2^{18}
Typed semantic-mass dimension	5
Traversal / global-context channel (TGC)	
Feature groups	$\mathbf{T}_0$, $\mathbf{T}_{1,\text{dep}}$, $\mathbf{T}_{1,\text{dry}}$, $\mathbf{T}_P$, $\mathbf{M}_1$
Dependency traversal depth	1 hop, direction-separated
Architectural position	PageRank, k-core
Feature scaling	raw and expanding-window z-score
z-score warm-up	30 commits
Tier extraction	once per project, cached
Stacking head	Logistic Regression
Penalty	ℓ_1, $C = 0.2$
Solver	`liblinear`
Class weighting	`balanced`
Feature standardization	`StandardScaler`
Baseline models	
Logistic Regression (LR)	
Penalty	ℓ_2
Class weighting	`balanced`
Histogram Gradient Boosting (HGB)	
Classifier	`HistGradientBoosting`
Class weighting	`balanced`
LApredict	
Classifier	Logistic Regression
Class weighting	`balanced`
JITLine	
Classifier	Random Forest
DeepJIT	
Optimizer	Adam
`embedding_dim`	64
`filter_sizes`	(1, 2, 3)
`num_filters`	64
`hidden_units`	512
`dropout_keep_prob`	0.5
`learning_rate`	10^{-4}
`l2_reg_lambda` / weight decay	10^{-5}
`epochs`	10

Table 6: Execution environments, hardware resources, and software versions used in the experiments.

Component / Resource	Value
KG-Commit execution environment	
Processor	Intel Core i7-13620H
CPU cores / threads	10 / 16
CPU base frequency	2.4 GHz
Memory	16 GB RAM
GPU usage	None (CPU-only)
KG-Commit software stack	
Python	3.13.5
Neo4j Community	2026.05
`neo4j` Python driver	6.2.0
Git	2.45.1
javalang	0.13.0
NumPy	2.2.6
SciPy	1.16.2
scikit-learn	1.7.2
pandas	2.3.2
networkx	3.5
DeepJIT execution environment	
Platform	Kaggle Notebook
Accelerator	NVIDIA Tesla T4
GPU compute capability	7.5 (`sm_75`)
DeepJIT software stack	
Python	3.12.13
PyTorch	2.10.0+`cu128`
CUDA runtime	12.8

pairwise Macro-F1 summary in Table 7 shows W/T/L records of 11/0/0 against RF, HGB, DeepJIT, and LR, 10/0/1 against LApredict, and 9/0/2 against JITLine-online. These differences are statistically significant across all six baselines. For G-Mean and AUC, the paired differences are also significant against the other five baselines, but not against JITLine-online ($p = .116$ and $p = .067$, respectively). The online evolution of Macro-F1 across the project streams is shown in Figure 9.

The effort-aware comparison with JITLine-online also favors KG-Commit (Table 8). KG-Commit achieves a higher Macro-Avg P_{opt} (0.889 versus 0.878) and ACC@20%LOC (0.653 versus 0.633), with W/T/L records of 9/1/1 and 10/0/1 respectively. The paired differences are statistically significant for both P_{opt} ($p = .004$) and ACC@20%LOC ($p = .002$). At the project level, the relative performance varies across the two measures, but the aggregate results indicate that KG-Commit's predictive gains remain evident when inspection effort is taken into account.

5.2. RQ2: Efficiency and Scalability

We compare the computational cost of processing each incoming commit in Table 9. For KG-Commit, routine per-commit processing includes graph ingestion, context retrieval, and prediction. For the baselines, it includes the corresponding featurization and prediction steps. Periodic model refitting is reported separately because it is triggered only every $M = 200$ commits.

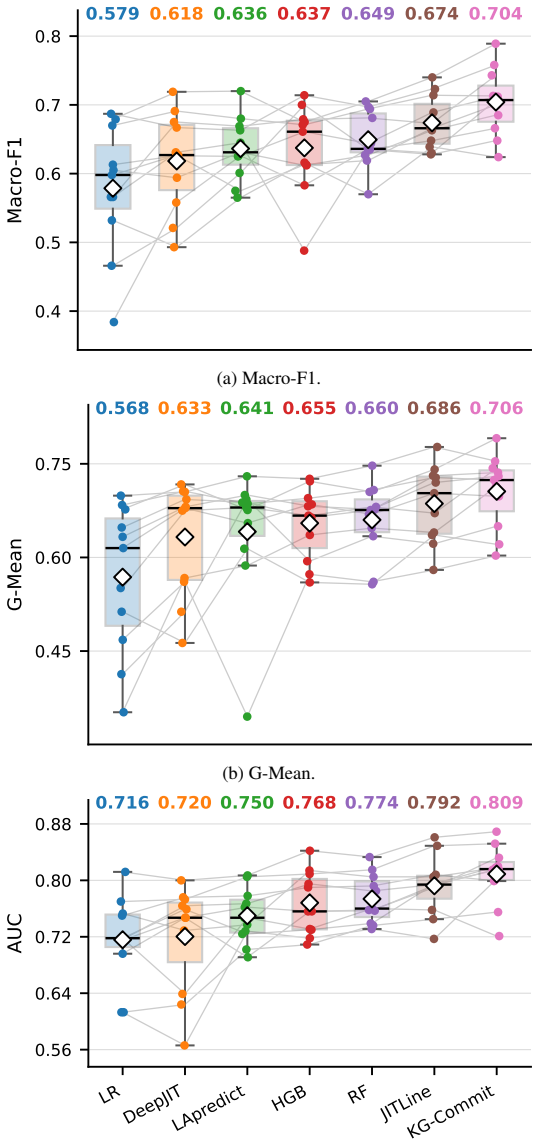

(a) Macro-F1.

(b) G-Mean.

(c) AUC.

Figure 8: Project-level distributions of the performance metrics under the online protocol. Each boxplot summarizes results over the 11 ApacheJIT projects (Section 4.2). Aggregate means are annotated above the boxplots, and individual project values are overlaid to show cross-project variation.

Table 7: Performance of KG-Commit and baselines under the online protocol (Section 4.4) over ApacheJIT projects (Section 4.2). The best model for each metric is shown in **bold** within every project and aggregate row. The final rows summarize pairwise differences between KG-Commit (F+G+T) and each baseline; W/T/L denotes project-level wins/ties/losses, and Wilcoxon p values are from two-sided paired tests over the 11 project scores.

Project	KG-Commit (F+G+T, S@200)			JITLine-online			RF			LApredict			HGB			DeepJIT			LR		
	Macro-F1	G-Mean	AUC	Macro-F1	G-Mean	AUC	Macro-F1	G-Mean	AUC	Macro-F1	G-Mean	AUC	Macro-F1	G-Mean	AUC	Macro-F1	G-Mean	AUC	Macro-F1	G-Mean	AUC
ActiveMQ	**0.712**	**0.730**	**0.816**	0.689	0.720	0.793	0.644	0.677	0.757	0.661	0.700	0.762	0.625	0.682	0.756	0.626	0.681	0.747	0.613	0.633	0.696
Camel	**0.685**	0.698	**0.832**	0.663	**0.703**	0.790	0.627	0.669	0.758	0.612	0.655	0.691	0.631	0.685	0.756	0.594	0.679	0.747	0.605	0.615	0.715
Cassandra	0.713	0.724	0.799	**0.714**	**0.728**	**0.808**	0.694	0.708	0.792	0.671	0.686	0.778	0.680	0.695	0.790	0.691	0.706	0.776	0.670	0.684	0.750
Flink	**0.758**	0.754	**0.852**	0.723	**0.777**	0.849	0.697	0.747	0.815	0.714	0.730	0.805	0.663	0.726	0.809	0.667	0.705	0.773	0.687	0.699	0.770
Groovy	**0.700**	**0.736**	**0.820**	0.666	0.731	0.795	0.619	0.676	0.739	0.613	0.688	0.724	0.575	0.664	0.730	0.627	0.693	0.759	0.598	0.648	0.718
HBase	**0.743**	**0.743**	**0.815**	0.673	0.671	0.794	0.681	0.681	0.785	0.679	0.680	0.767	0.669	0.667	0.795	0.675	0.675	0.764	0.566	0.551	0.716
Hive	**0.666**	**0.603**	**0.818**	0.648	0.580	0.805	0.635	0.561	0.805	0.488	0.345	0.737	0.645	0.573	0.814	0.631	0.561	0.729	0.566	0.468	0.753
Kafka	**0.789**	**0.791**	**0.869**	0.740	0.741	0.861	0.705	0.705	0.833	0.675	0.676	0.807	0.720	0.722	0.842	0.719	0.717	0.800	0.679	0.677	0.812
Spark	0.624	0.621	0.721	**0.639**	**0.636**	0.758	0.570	0.557	**0.760**	0.616	0.614	0.747	0.565	0.560	0.731	0.493	0.463	0.639	0.532	0.513	0.718
Zeppelin	0.648	0.650	**0.755**	0.628	0.622	0.745	0.635	0.634	0.736	**0.700**	**0.693**	0.702	0.601	0.594	0.709	0.521	0.513	0.624	0.466	0.413	0.613
Zookeeper	**0.707**	**0.714**	**0.802**	0.630	0.640	0.717	0.636	0.647	0.731	0.583	0.587	0.728	0.626	0.636	0.718	0.558	0.567	0.566	0.384	0.352	0.613
Macro-Avg	**0.704**	**0.706**	**0.809**	0.674	0.687	0.792	0.649	0.660	0.774	0.637	0.641	0.750	0.636	0.655	0.768	0.618	0.633	0.720	0.579	0.568	0.716
Micro-Avg	**0.709**	**0.713**	**0.823**	0.680	0.704	0.803	0.653	0.676	0.777	0.637	0.652	0.743	0.641	0.674	0.775	0.633	0.670	0.751	0.612	0.613	0.729
Mean Δ		–		+.030	+.020	+.017	+.055	+.046	+.035	+.067	+.065	+.059	+.068	+.051	+.041	+.086	+.073	+.089	+.125	+.137	+.093
W/T/L		–		9/0/2	7/0/4	9/0/2	11/0/0	11/0/0	10/0/1	10/0/1	10/0/1	10/0/1	11/0/0	11/0/0	10/0/1	11/0/0	11/0/0	11/0/0	11/0/0	11/0/0	11/0/0
Wilcoxon p		–		.005	.116	.067	< .001	< .001	.019	.010	.011	.003	< .001	< .001	.005	< .001	< .001	< .001	< .001	< .001	< .001

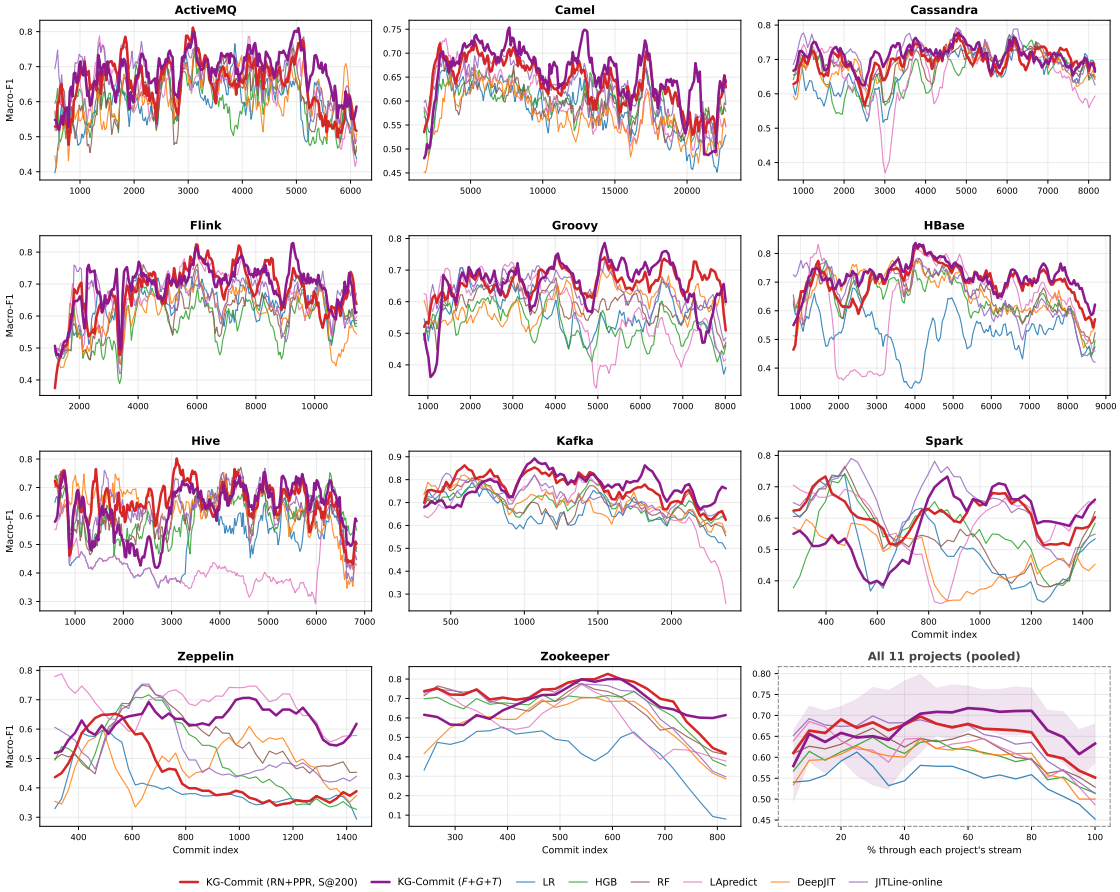

Figure 9: Running online Macro-F1 of KG-Commit compared with the online implementation of baselines. The rolling window is w=150 at stride 25.

Table 8: Effort-aware comparison of KG-Commit and JITLine-online. For each KG-Commit result, parentheses report the absolute difference from JITLine-online. The best value for each metric is shown in **bold**. The final rows summarize project-level differences, wins/ties/losses, and two-sided paired Wilcoxon tests over the 11 projects.

Project	KG-Commit(F+G+T)		JITLine-online	
	P_{opt}	ACC@20	P_{opt}	ACC@20
ActiveMQ	**0.857** (.010↑)	**0.624** (.023↑)	0.847	0.601
Camel	**0.837** (.024↑)	**0.625** (.034↑)	0.813	0.591
Cassandra	**0.914** (.000=)	**0.696** (.003↑)	**0.914**	0.693
Flink	**0.860** (.007↑)	**0.591** (.005↑)	0.853	0.586
Groovy	**0.863** (.013↑)	**0.678** (.035↑)	0.850	0.643
HBase	**0.927** (.007↑)	**0.716** (.010↑)	0.920	0.706
Hive	0.952 (.002↓)	0.737 (.001↓)	**0.954**	**0.738**
Kafka	**0.907** (.007↑)	**0.632** (.008↑)	0.900	0.624
Spark	**0.841** (.004↑)	**0.531** (.014↑)	0.837	0.517
Zeppelin	**0.915** (.012↑)	**0.682** (.028↑)	0.903	0.654
Zookeeper	**0.901** (.030↑)	**0.676** (.065↑)	0.871	0.611
Macro-Avg	**0.889** (.011↑)	**0.653** (.020↑)	0.878	0.633
Micro-Avg	**0.877** (.012↑)	**0.653** (.019↑)	0.865	0.634
Mean Δ	–	–	+.010	+.020
W/T/L	–	–	9/1/1	10/0/1
Wilcoxon p	–	–	.004	.002

KG-Commit's routine cost is dominated by graph ingestion, with a median of approximately 1.33 s per commit. The isolated graph-retrieval and F_{ov} = RN+PPR inference components require only 0.116 ms and 0.325 ms respectively. The added TGC values in Section 3.3.6 are cached and read as a compact feature vector (Appendix E); they do not introduce an additional full-graph Neo4j traversal. The evaluated baselines require approximately 7.9–8.5 ms per commit before periodic refitting. KG-Commit therefore incurs higher per-commit computation in exchange for maintaining rich project-wide context. Whether this additional cost is operationally important depends on the rate at which commits arrive. As discussed in Section 6.2, the observed commit arrival time is much larger than KG-Commit's processing time across all 11 projects.

Table 9: Median runtime costs across all projects. Routine processing includes the work performed for every incoming commit. Periodic refit is reported separately and amortized over M = 200 commits. *Feat.*, *retr.*, and *pred.* denote featurization, retrieval, and prediction. *Includes computation of the 12 change metrics.

	KG-Commit	LR	HGB	RF	LA predict	DeepJIT	JITLine online
Routine per-commit processing (ms/commit)							
Ingest	1,330	–	–	–	–	–	–
Feat.	–	7.912*	7.912*	7.912*	7.885	7.912*	8.213
Retr.	0.116	–	–	–	–	–	–
Pred.	0.325	0.001	0.009	0.245	0.001	0.363	0.298
Total	**≈1,330.44**	7.913	7.921	8.157	7.886	8.275	8.511
Periodic refit (amortized over M = 200 commits)							
Refit	1.05	0.04	2.83	2.08	0.02	53.04	9.85

Table 10 reports the graph scale, inference latency, and ingest cost of KG-Commit for each project. Graph-inference component F_{ov}=RN+PPR, has a median inference time of 0.325 ms and a median p_{95} of 0.399 ms. The overall runtime of KG-Commit is instead dominated by graph ingestion, whose median cost is approximately 1.33 s per commit. DeepWalk and KGE are faster to apply, at approximately 0.001 ms, but require periodic refitting, whereas RN and PPR operate directly on the graph. The AST delta is highly skewed: the median commit changes 282 edges, compared with 5,107 at the p_{95}, with a Gini coefficient of 0.78. Ingest cost is therefore driven mainly by a small number of large commits rather than the accumulated project history.

Lifecycle and Scaling. Figure 10 shows how the graph and its deployment costs grow with project history. Figure 10a shows the accumulated edges, while Figure 10b and Figure 10c show that per-commit work does not increase with it. In the final fifth of Camel's history, the median AST delta and ingest time are 0.55× and 0.86× their values in the first fifth, and median ingest time remains approximately 1.16 s. Ingest cost therefore depends mainly on the incoming change instead of the existing graph size. Figure 10d and Figure 10e show that soft deletion preserves historical structure while storage grows linearly. Figure 10f and the corresponding analyses of the other projects show the same trends. We present Camel because it is the most demanding case, with 22,695 commits, 12.4 million cumulative AST edges, and an estimated footprint of 699 MB.

5.3. RQ3: Contribution of KG-Commit Layers to Predictive Performance

Table 11 examines the contribution of KG-Commit's representation layers while holding inference fixed at F_{ov}. The graph is progressively enriched from Core to AST and then CSTG, so differences in performance reflect changes in the representation itself. Layer 2 provides little benefit under F_{ov}, whereas adding CSTG consistently improves F_{ov} results across all projects, increasing the median Macro-F1 from 0.552 for Core to 0.644 for CSTG. The same pattern can be seen throughout the commit stream in Figure 11 and across projects in Figure 12.

The limited gain from AST suggests that the generic inference methods in Section 3.3.5 do not fully exploit its fine-grained structure. CSTG, in contrast, introduces semantic entities and relations that are more accessible to RN and PPR. This result is separate from the CSTG feature channel G and the traversal/global-context feature block T, which augment the graph-based inference

Table 10: Internal cost profile of KG-Commit by project. N_c is the number of commit nodes, and *c/s* is the processing throughput in commits per second. The inference columns isolate the five projection-based graph channels and F_{ov} = RN+PPR (Section 3.3.6); F-p_{95} is the 95th-percentile latency of this graph component. The TGC block used by the final F_{ov}+G+T configuration is cached separately (Appendix E). Under INGEST, *ms* is graph-update time per commit, *edges* is the total AST delta (Section 3.3.3), and p_{50}, p_{95}, and Gini describe the AST-delta distribution.

	GRAPH		INFERENCE time (ms/commit)							INGEST & per-commit AST delta				
	N_c	c/s	RN	PPR	LP	DW	KGE	F_{ov}	Fp95	ms	edges	p50	p95	Gini
ActiveMQ	6,126	3,080	0.078	0.247	0.027	0.001	0.001	**0.325**	0.399	1,277	3.27M	97	1,848	0.80
Camel	22,695	740	0.362	0.989	0.100	0.002	0.001	**1.352**	1.509	1,163	12.38M	133	2,044	0.78
Cassandra	8,159	1,691	0.152	0.440	0.046	0.001	0.001	**0.591**	0.775	1,519	11.84M	283	6,438	0.78
Flink	11,459	1,066	0.242	0.697	0.069	0.001	0.001	**0.938**	1.078	1,330	16.67M	371	6,515	0.75
Groovy	8,059	3,219	0.103	0.208	0.038	0.001	0.000	**0.311**	0.367	823	3.61M	84	1,464	0.83
HBase	8,727	1,547	0.161	0.485	0.049	0.001	0.001	**0.646**	0.796	1,648	14.01M	293	6,578	0.81
Hive	6,842	1,846	0.133	0.409	0.041	0.001	0.001	**0.542**	0.677	2,177	12.20M	383	7,621	0.79
Kafka	2,384	5,855	0.046	0.124	0.016	0.001	0.001	**0.171**	0.336	2,324	3.17M	375	6,083	0.74
Spark	1,465	14,022	0.017	0.054	0.010	0.001	0.001	**0.071**	0.088	1,238	0.82M	153	2,310	0.76
Zeppelin	1,451	11,652	0.023	0.063	0.011	0.001	0.001	**0.086**	0.116	1,243	1.63M	213	5,107	0.79
Zookeeper	839	18,494	0.015	0.039	0.008	0.001	0.001	**0.054**	0.062	1,497	0.78M	282	3,917	0.72
Median	6,842	3,080						**0.325**		1,330				0.78

through F+G and F+G+T, shown in Figure 11 and Figure 12.

The four Layer-2 alternatives perform similarly, and their ordering varies across projects (Table 11). Among these Layer-2 candidates, we select AST because its incremental delta can be computed using canonical subtree hashing (Section 3.3.3), whereas alternative choices require an ordinal fallback matcher (Appendix A). AST also contains more nodes and edges (Section 5.2, Figure 10a), potentially capturing richer structures that F_{ov} may not fully exploit, a limitation we revisit in Section 6.6.

Performance also varies across projects and inference methods. For example, Macro-F1 for F_{ov} with CSTG ranges from 0.525 on Zeppelin to 0.723 on Kafka (Table 11). The results can vary across the individual inference methods, with Cassandra ranging from 0.327 for LP to 0.643 for KGE (see Appendix B). We study the differences among inference channels in Section 5.4.

5.4. RQ4: Inference Channels and Fusion

PPR provides the strongest single-channel Macro-F1 of .643, as shown in Table 12. Combining additional channels brings modest gains, with the best fusion reaching 0.653. We fixed F_{ov} = RN+PPR before computing these aggregate results with the rationale of combining RN's local neighborhood evidence with PPR's global propagation (Section 3.3.5), hence avoiding any advantage from project-specific fusion tuning. The performance cost is small, as F_{ov} achieves 0.641 Macro-F1, only 0.012 below the best, while remaining competitive in G-Mean and AUC. Additionally, RN and PPR are computed directly from the graph topology and require no fitting, periodic refitting, random initialization, or seed control, unlike fusions that include learned embedding channels. Consequently, F_{ov} is reproducible and cheap to serve with a median inference cost of 0.325 ms per commit.

Figure 13 illustrates how F_{ov} and G complement each other. Their fusion raises mean Macro-F1 to 0.676, compared with 0.641 for F_{ov} and 0.646 for G alone. S@200 slightly improves the mean further to 0.681 and narrows the central spread, although its main benefit is during cold start, when it delays the CSTG channel until the project has accumulated 200 commits (see Section 6.3). Adding T further increases the mean Macro-F1 to 0.704, giving the highest performance among the evaluated configurations.

6. Discussion

6.1. On the Necessity of Realistic Online Evaluation

Some JIT-SDP studies use conventional cross-validation (Qiao and Wang, 2019), which does not preserve the chronological order of commits. Accordingly, such time-agnostic splitting can allow later commits to appear in the training data when earlier commits are used for testing, potentially leading to optimistic performance estimates, as shown in Table 13. Other studies adopt time-aware evaluation (McIntosh and Kamei, 2018; Pornprasit and Tantithamthavorn, 2021; Pornprasit et al., 2021), where earlier commits are used for training and later commits for testing. Although this preserves temporal order, the model is typically fixed

Table 11: Online performance across all 11 projects under fusion F_{ov}. Columns follow the KG-Commit hierarchy: Core (Layer 1, Section 3.3.2), four within-file graph representations (Layer 2, Section 3.3.3), and CSTG (Layer 3, Section 3.3.4). **Bold** values mark the best representation for each project and metric.

Project	Layer 1			Layer 2: within-file subgraph												Layer 3		
	Core			+AST			+CFG			+DFG			+PDG			+CSTG		
	F_1	G	AUC	F_1	G	AUC	F_1	G	AUC	F_1	G	AUC	F_1	G	AUC	F_1	G	AUC
`ActiveMQ`	.572	.636	.697	.565	.649	.721	.558	.643	.717	.551	.637	.718	.551	.637	.718	**.642**	**.706**	**.778**
`Camel`	.579	.668	.725	.595	.684	.743	.603	.689	.754	.610	.687	.764	.599	.692	.754	**.637**	**.730**	**.792**
`Cassandra`	.552	.559	.660	.583	.591	.685	.581	.590	.681	.584	.592	.691	.580	.588	.680	**.644**	**.658**	**.749**
`Flink`	.647	.637	.742	.607	.654	.753	.614	.651	.741	.606	.646	.733	.616	.653	.741	**.685**	**.731**	**.818**
`Groovy`	.596	.649	.721	.566	.661	.748	.593	.679	.747	.598	.678	.738	.594	.681	.747	**.656**	**.729**	**.801**
`HBase`	.503	.465	.678	.593	.579	.732	.640	.638	.733	.627	.622	.735	.626	.621	.732	**.679**	**.680**	**.793**
`Hive`	.520	.412	.640	.554	.456	.691	.565	.474	.689	.558	.461	.679	.581	.498	.689	**.638**	**.573**	**.769**
`Kafka`	.619	.618	.686	.602	.585	.712	.688	.686	.746	.661	.655	.734	.685	.684	.745	**.723**	**.724**	**.809**
`Spark`	.439	.392	.630	.380	.309	.517	.490	.454	.614	.420	.357	.583	.465	.420	.602	**.574**	**.566**	**.666**
`Zeppelin`	.478	.422	.590	.450	.382	.634	.461	.412	.615	.410	.344	.608	.443	.387	.611	**.525**	**.491**	**.654**
`Zookeeper`	.543	.551	.637	.511	.499	.521	.511	.492	.584	.506	.486	.626	.503	.481	.583	**.651**	**.661**	**.683**

Table 12: All 31 fixed fusion combinations across the 11 projects. Each cell reports the project-level mean ± the half-width of its Student-t 95% confidence interval. The fixed overall fusion F_{ov} = RN+PPR is highlighted in gray.

Combination	Macro-F1	G-Mean	AUC
LP	.446 ± .064	.433 ± .103	.632 ± .047
RN	.410 ± .040	.383 ± .071	.593 ± .039
DW	.600 ± .039	.619 ± .049	.691 ± .031
KGE	.609 ± .031	.623 ± .050	.688 ± .038
PPR	.643 ± .033	.652 ± .050	.758 ± .025
RN+LP	.553 ± .067	.562 ± .088	.695 ± .063
LP+KGE	.578 ± .059	.587 ± .085	.698 ± .068
RN+KGE	.572 ± .063	.579 ± .090	.685 ± .072
LP+DW	.605 ± .045	.627 ± .061	.712 ± .051
RN+DW	.599 ± .044	.621 ± .058	.706 ± .042
PPR+LP	.632 ± .034	.651 ± .052	.744 ± .046
DW+KGE	.623 ± .043	.635 ± .057	.707 ± .044
PPR+KGE	.648 ± .025	.661 ± .042	.744 ± .029
RN+PPR	.641 ± .036	.659 ± .055	.756 ± .040
PPR+DW	.649 ± .038	.663 ± .050	.739 ± .037
RN+LP+KGE	.575 ± .063	.582 ± .089	.708 ± .064
RN+LP+DW	.609 ± .048	.629 ± .064	.718 ± .050
LP+DW+KGE	.619 ± .046	.634 ± .063	.722 ± .055
RN+DW+KGE	.615 ± .045	.631 ± .061	.723 ± .048
PPR+LP+KGE	.635 ± .035	.651 ± .054	.745 ± .045
RN+PPR+LP	.640 ± .041	.656 ± .057	.754 ± .044
RN+PPR+KGE	.640 ± .035	.656 ± .054	.754 ± .039
PPR+LP+DW	.644 ± .039	.664 ± .054	.748 ± .044
PPR+DW+KGE	.651 ± .037	.663 ± .051	.744 ± .039
RN+PPR+DW	.652 ± .039	.670 ± .052	.754 ± .041
RN+LP+DW+KGE	.617 ± .048	.631 ± .066	.729 ± .053
RN+PPR+LP+KGE	.640 ± .041	.652 ± .058	.754 ± .044
PPR+LP+DW+KGE	.646 ± .039	.662 ± .056	.750 ± .045
RN+PPR+LP+DW	.650 ± .042	.667 ± .056	.756 ± .044
RN+PPR+DW+KGE	.653 ± .038	.670 ± .052	.756 ± .042
RN+PPR+LP+DW+KGE	.652 ± .042	.667 ± .056	.758 ± .044

throughout an entire train/test block. Such an evaluation requires a sufficiently large historical training block, making it unsuitable for projects in the early-to-mid development cycle. It also does not reproduce the per-commit processing and maintenance cycle of a deployed system or account for label-verification latency through the gap parameter (Tan et al., 2015; Gomes Cabral et al., 2019; Song and Minku, 2023; Cabral and Minku, 2023). Consequently, challenges such as delayed feedback and concept drift remain largely unexamined (McIntosh and Kamei, 2018; Cabral and Minku, 2023). Block-based evaluation also cannot reveal potential catastrophic forgetting that may arise under sequential updating (Cabral and Minku, 2023; Kirkpatrick et al., 2017).

In our comparison, block-based time-aware evaluation underestimates performance (Table 13) since holding the model fixed over many commits prevents continual refitting and adaptation as the project evolves. To capture this adaptation while avoiding temporal leakage, we use the online protocol described in Section 4.4, which reflects the deployment constraints in Section 3.2.2. Its small warm-up ratio of .05 also enables evaluation from the early stages of a project.

Table 13: Mean baseline performance across 11 projects under online, block-based time-aware, and random evaluation.

	Macro-F1			G-Mean			AUC		
Model	**On.**	**Off.**	**Rand.**	**On.**	**Off.**	**Rand.**	**On.**	**Off.**	**Rand.**
LR	.579	.542	.655	.568	.579	.661	.716	.706	.754
HGB	.636	.583	.720	.655	.623	.707	.768	.747	.810
LApredict	.637	.596	.667	.641	.643	.679	.750	.775	.769

6.2. *Per-Commit Cost Relative to Commit Arrival Time*

The practical suitability of KG-Commit depends on whether its per-commit processing cost is compatible

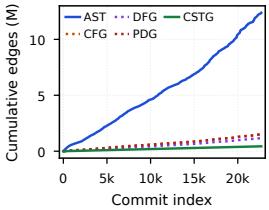

(a) Cumulative edges by representation.

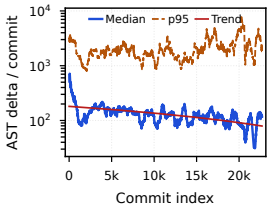

(b) Rolling median, p95, and trend of the per-commit AST delta.

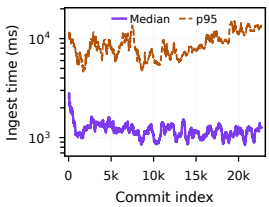

(c) Rolling median and p95 per-commit ingest time.

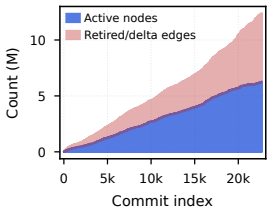

(d) Active and retired graph structure.

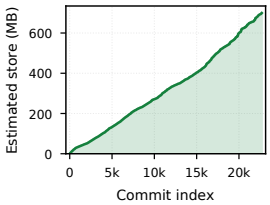

(e) Estimated graph-store footprint.

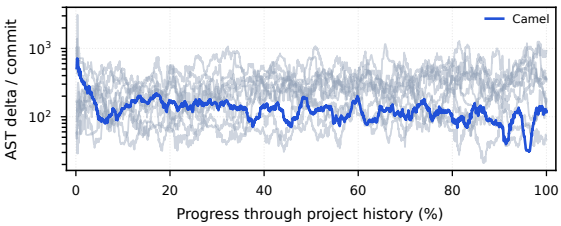

(f) Rolling-median AST delta across all 11 projects. Camel is highlighted.

Figure 10: Lifecycle and scaling of KG-Commit. Figure 10a–10e report Camel, the largest project history. Figure 10f compares normalized per-commit AST deltas across all 11 projects.

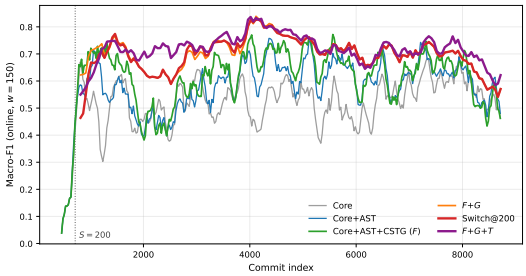

Figure 11: Online Macro-F1 by representation layer on HBase. The curves compare Core, Core+AST, Core+AST+CSTG, along with the fusions F_{ov}, F_{ov}+G, S@200 policy, and F_{ov}+G + T. The dotted line marks the switch point S =200.

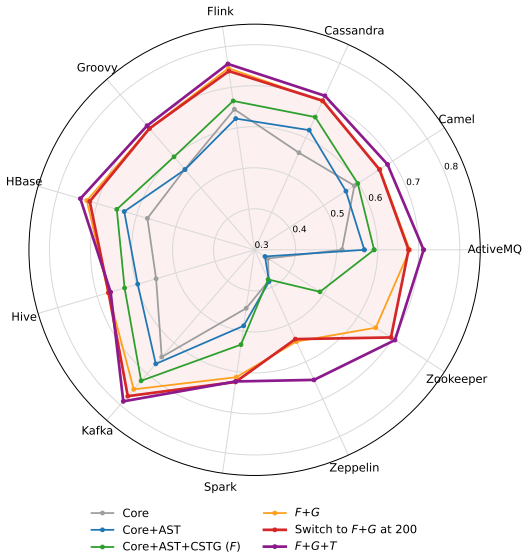

Figure 12: Macro-F1 score by KG-Commit representation layer across all 11 projects, together with the corresponding additional configurations in Section 3.3.6.

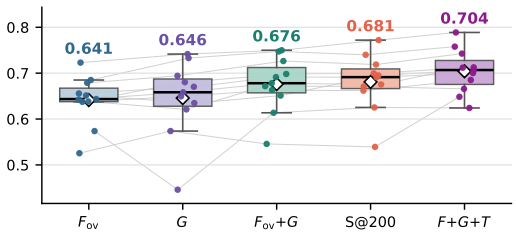

Figure 13: Project-level Macro-F1 for F_{ov}, G, F_{ov}+G, S@200 policy, and F_{ov}+G + T. Boxes show the interquartile range, horizontal lines the medians, diamonds the means, and points the projects; faint lines connect results from the same project.

with the rate at which commits arrive in practice. KG-Commit requires approximately 1.33 s to process an incoming commit (Section 5.2), with most of this cost arising from the incremental graph update. Table 14 reports the observed intervals between consecutive commits across the projects. Even among closely spaced commits, the shortest lower-tail interval is 8.0 s on Cassandra, while the corresponding intervals for the remaining projects range from 25 s to more than 27 min. Median commit spacing is considerably larger, ranging from 1.20 h on Camel to 45.55 h on Zookeeper. These observations indicate that KG-Commit's per-commit processing cost is compatible with the commit arrival rates observed in the evaluated projects.

Table 14: Commit arrival time across all 11 projects. Mean, standard deviation (SD), median, and P95 are reported in hours, while P05 is reported in seconds to expose short intervals between consecutive commits.

Project	**Mean ± SD (h)**	**Median (h)**	**P05 (s)**	**P95 (h)**
ActiveMQ	20.03 ± 44.95	4.23	117.2	90.15
Camel	4.93 ± 9.95	1.20	114.0	20.79
Cassandra	11.57 ± 24.93	2.88	8.0	53.38
Flink	6.77 ± 17.86	1.32	25.0	26.45
Groovy	17.72 ± 37.57	4.59	105.0	77.56
HBase	12.77 ± 20.93	5.34	301.2	50.60
Hive	14.45 ± 30.73	5.21	306.0	61.66
Kafka	30.18 ± 189.05	8.67	574.7	88.45
Spark	54.22 ± 377.47	19.19	1664.6	162.21
Zeppelin	38.37 ± 77.34	16.08	360.6	147.91
Zookeeper	126.30 ± 218.03	45.55	429.7	501.36

6.3. S@200 Switching and Cold-Start Improvement

Unlike the inference channel F, the CSTG channel G is not equally useful from the start. It learns from the vocabulary accumulated in commit messages and diffs (Section 3.3.4), so after a short warm-up, its term and co-occurrence statistics may still be too sparse for stable predictions. On the other hand, F operates on graph topology (Section 3.3.5) and does not depend on a fitted vocabulary. The two channels also capture fundamentally different patterns, which may explain why their combination performs better in Figure 13. We therefore use F_{ov} for the first 200 commits (after warm-up) and add G when more project-specific language has accumulated. On both Spark (Figure 14a) and Zookeeper (Figure 14b), S@200 avoids the weaker early performance of F+G and stays ahead through much of the later stream, even after G is introduced, so the early choice of channel appears to shape later adaptation. Noisy G channel scores from cold start can carry over into subsequent updates, whereas starting with F_{ov} gives later predictions a cleaner history.

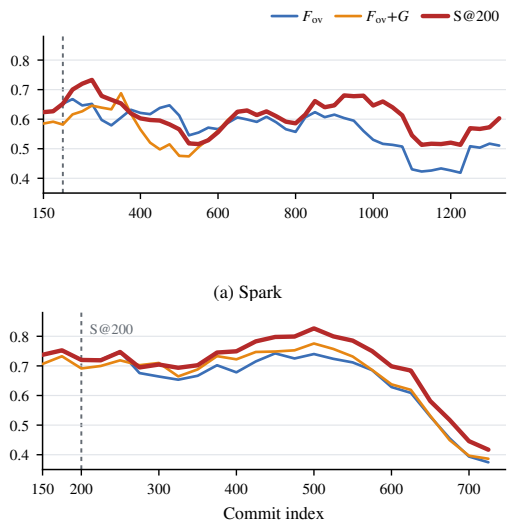

Figure 14: Effect of S@200 on Spark and Zookeeper. Curves report 150 rolling Macro-F1 with a stride of 25 commits; the displayed sequences therefore begin at the first complete window, at commit index 150.

6.4. Sensitivity of the Online Protocol to Operational Constraints and Hyperparameters

We study KG-Commit's sensitivity to the operational constraints of the online protocol and to the choice of refit interval M and switching point S (Section 4.4). The warm-up ratio K and verification gap g determine how much historical information is available and when labels become observable (Section 3.2.2). These sensitivity experiments use F_{ov}+G under the S@200 policy. This isolates the effects of the online protocol and its hyperparameters from the additional traversal/global-context features in T. The selected values are subsequently used unchanged in the final F_{ov}+G+T configuration.

We test $K \in \{0.05, 0.10, 0.20, 0.30, 0.40, 0.50\}$ and $g \in \{0, 10, 25, 50, 100, 200\}$. Macro-F1 remains stable across K for most projects, with the largest variation occurring in the smaller Spark, Zeppelin, and Zookeeper histories. It is even less sensitive to g, whose curves are nearly flat except for a modest change on Zookeeper. We also test $M \in \{25, 50, 100, 200\}$ and $S \in \{0, 100, 200, 250, 300, 400, 500, 600, 750, 1K, 1.5K, 2K, 3K, \infty\}$, where project history permits. Most projects remain stable across M, while the larger changes at M=200 again occur in smaller projects. Performance also changes little for S between 200 and 500. Moving from S=0 to S=200, however, improves Macro-F1 by 0.012 on Spark and 0.044 on Zookeeper, consistent

with the effect discussed in Section 6.3.

The values used in our main experiments (Section 5) were fixed before obtaining the sensitivity results in Figure 15. They were chosen for practical deployment instead of aiming to maximize performance on each project. Using K=0.05 allows KG-Commit to begin predicting after only 5% of the project history, although it trails the best tested K by 0.064 on Spark and 0.117 on Zookeeper. On most other projects, the choice of K has little effect. We similarly choose the largest refit interval, M=200, to reduce how often refitting occurs. This setting lowers Macro-F1 on some smaller projects, most clearly on Zeppelin, Zookeeper, and Spark, where performance decreases by 0.168, 0.089, and 0.057 relative to M=25. Lowering M would trigger refitting more frequently and increase its amortized C_{refit}/M cost. The selected setting therefore trades some performance on smaller projects for less frequent refitting, making our reported results for S@200 conservative.

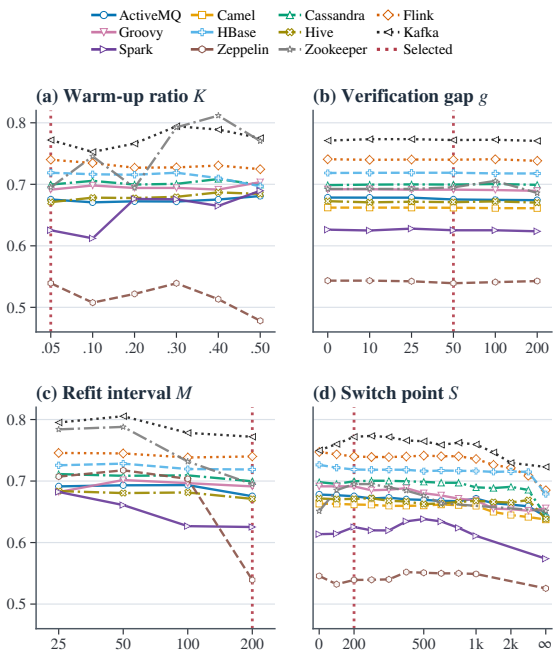

Figure 15: Macro-F1 sensitivity of the F_{ov}+G configuration to the warm-up ratio K, verification gap g, refit interval M, and switch point S. Dotted lines mark the selected settings K=0.05, g=50, M=200, and S=200.

6.5. Online Threshold Adaptation

KG-Commit uses the default threshold of 0.5 for the first 300 evaluated commits and then re-estimates it every 150 commits by maximizing Macro-F1 over the labels available at that point (Section 4.4). The updated value is used from the next commit onward. As shown in Figure 16, the resulting operating point varies across projects. Cassandra and HBase remain close to 0.5, whereas Camel, Flink, and Groovy move toward higher thresholds. Hive, Kafka, Spark, Zeppelin, and Zookeeper instead settle below 0.5. Final thresholds range from 0.251 on Hive to 0.748 on Flink. A fixed cutoff would therefore impose different precision-recall trade-offs across projects. Periodic threshold tuning allows KG-Commit to adapt its decisions as the project's score and class distributions evolve, without refitting the underlying scoring model.

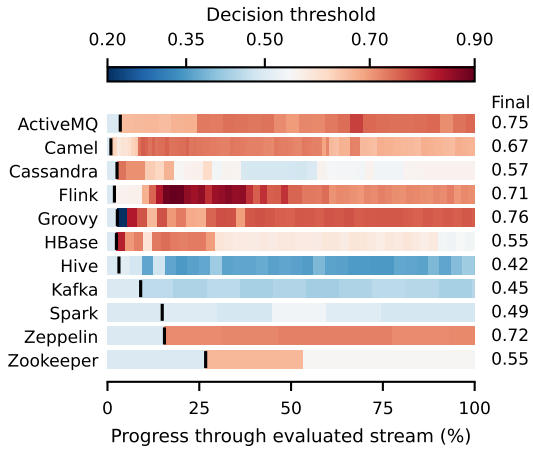

Figure 16: Online decision thresholds across the evaluated commit streams. Color indicates the threshold in force, black marks the first retuning after 300 evaluated commits, and the final threshold is reported on the right.

6.6. Limitations and Future Work

KG-Commit currently runs entirely on CPU. This keeps deployment inexpensive but restricts the complexity of graph inference. The evaluated inference channels use mostly generic graph projections and are not customized to consider specific node types, relations, or more informative regions for the purpose of JIT-SDP. The T channel exposes selected dependency, package, and graph-global context, but other aspects of the graph may remain unexploited, particularly fine-grained AST structure and richer typed or higher-order relational patterns. Therefore, although KG-Commit outperforms all evaluated baselines in predictive performance, the reported results should be viewed as a conservative estimate of what its representation can support under the current inference design, rather than as an upper bound on KG-Commit's inherent capability.

Furthermore, the current implementation is limited to Java because AST construction and delta extraction rely on `javalang`. Extending KG-Commit to other programming languages would require corresponding parsers and language-specific handling of source-code structure. In addition, each evaluated project is represented as a single repository. The current graph construction therefore does not model cross-repository dependencies or projects whose development history is distributed across multiple repositories.

Future work can examine other inference methods such as R-GCN, CompGCN, and HGT, together with projections designed around the entities and relations most relevant to a target commit for defect prediction. GPU-based inference can also make broader graph context practical, provided that the resulting end-to-end per-commit processing cost remains compatible with the commit rates expected in online JIT-SDP. Taken together, these directions suggest that the current results capture only an initial use of KG-Commit's representational capacity. Considerable room remains to exploit KG-Commit through richer inference and better graph projections. Beyond this, KG-Commit itself can be extended with additional information (e.g., caller/callee relations) to capture forms of project context not represented in the current design.

7. Threats to Validity

We discuss potential threats that may affect the credibility and generalizability of our results, grouped into internal, external, and construct validity.

7.1. Internal Validity

Temporal leakage is the main internal concern. The online protocol admits the current commit's unlabeled information but restricts labels and learned components to information available at prediction time (Section 4.4). Baselines were adapted to the same protocol which may introduce implementation differences. We mitigate these risks through a common stream, fixed settings, and the reported sensitivity analyses.

7.2. External Validity

The evaluation uses projects from the Apache open-source ecosystem, so the observed performance may not transfer to projects with different development processes or defect distributions. Evaluating KG-Commit on industrial and other open-source repositories is needed to establish broader generalizability.

7.3. Construct Validity

ApacheJIT uses an SZZ-based procedure to identify bug-inducing commits, and these labels may contain incorrect or missing links (Section 4.2). KG-Commit also relies on heuristic choices in both the AST (Section 3.3.3) and CSTG layers (Section 3.3.4). The AST layer uses heuristic matching to align nodes across edits, while CSTG uses rule-based term extraction, intent assignment, and term grounding. Moreover, efficiency and scalability are measured using execution time under the reported hardware and software environment, so absolute timings may differ on other systems.

8. Conclusion

This paper addressed a practical limitation of online JIT-SDP by making broader project context available at a computational cost compatible with real commit streams. KG-Commit maintains this context incrementally in an evolving knowledge graph. Its three layers capture repository history, within-file code structure, and commit semantics, while AST deltas maintain fine-grained changes through file evolution. The final $F_{\text{ov}}+G+T$ predictor additionally incorporates traversal/global context from the full graph. Across 11 Apache projects, this configuration achieves the highest aggregate Macro-F1 (0.704), G-Mean (0.706), and AUC (0.809). Under a realistic online protocol, KG-Commit outperforms LR, HGB, RF, and DeepJIT on all 11 projects, LApredict on 10, and JITLine-online on 9 projects in Macro-F1, with the aggregate paired difference statistically significant in every case.

KG-Commit processes each commit in approximately 1.33 s on CPU, with graph ingestion accounting for most of this cost. Lifecycle analysis shows that this per-commit processing remains stable as project history and graph size grow. Moreover, KG-Commit's processing time remains well below the observed time between consecutive commits. These results indicate that the computational cost of maintaining rich project context can be practical under the commit rates observed in real-world software projects. The current results are obtained using lightweight, CPU-only inference channels. Hence, they should be viewed as a conservative estimate of KG-Commit's potential. This leaves considerable room for richer inference methods to better exploit KG-Commit's representational capacity and make fuller use of the global structural and relational information maintained throughout project evolution.

9. Declarations

9.1. Funding

This research received no external funding.

9.2. Ethical approval

Ethical approval: Not applicable.

9.3. Informed consent

Informed consent: Not applicable.

9.4. Data Availability Statement

The datasets generated and/or analyzed during the current study are available at:

- **Data repository:**
  - Graph Dumps: https://zenodo.org/records/22348686
  - ApacheJIT Dataset: https://zenodo.org/records/5907002
- **Code repository:** https://github.com/Knowledge4Software/kg-commit

9.5. Conflict of Interest

The authors declare that they have no conflict of interest.

9.6. Clinical trial number

Clinical trial number: Not applicable.

10. Declaration of generative AI and AI-assisted technologies in the manuscript preparation process

During the preparation of this work, the authors used ChatGPT (OpenAI), using GPT-5.6 Sol, to improve the language, clarity, organization, and visual presentation of the manuscript, including the presentation of figures and other manuscript elements. After using this tool, the authors reviewed and edited the content as needed and take full responsibility for the content of the published article.

References

Abu Talib, M., Bou Nassif, A., Azzeh, M., Alesh, Y., Afadar, Y., 2024. Parameter-efficient fine-tuning of pre-trained code models for just-in-time defect prediction. Neural Computing and Applications 36, 16911–16940. doi:10.1007/s00521-024-09930-5.

Allamanis, M., Brockschmidt, M., Khademi, M., 2018. Learning to represent programs with graphs, in: International Conference on Learning Representations (ICLR).

Alon, U., Brody, S., Levy, O., Yahav, E., 2019a. code2seq: Generating sequences from structured representations of code, in: International Conference on Learning Representations (ICLR).

Alon, U., Zilberstein, M., Levy, O., Yahav, E., 2019b. code2vec: Learning distributed representations of code. Proceedings of the ACM on Programming Languages 3, 1–29. doi:10.1145/3290353.

Angles, R., Arenas, M., Barceló, P., Hogan, A., Reutter, J., Vrgoč, D., 2017. Foundations of modern query languages for graph databases. ACM Computing Surveys 50, 1–40. doi:10.1145/3104031.

Batagelj, V., Zaversnik, M., 2003. An o(m) algorithm for cores decomposition of networks. URL: https://arxiv.org/abs/cs/0310049, arXiv:cs/0310049.

Belkin, M., Niyogi, P., Sindhwani, V., 2006. Manifold regularization: A geometric framework for learning from labeled and unlabeled examples. Journal of Machine Learning Research 7, 2399–2434.

Bollacker, K., Evans, C., Paritosh, P., Sturge, T., Taylor, J., 2008. Freebase: A collaboratively created graph database for structuring human knowledge, in: Proceedings of the 2008 ACM SIGMOD International Conference on Management of Data (SIGMOD), pp. 1247–1250. doi:10.1145/1376616.1376746.

Bordes, A., Usunier, N., Garcia-Durán, A., Weston, J., Yakhnenko, O., 2013. Translating embeddings for modeling multi-relational data, in: Advances in Neural Information Processing Systems (NeurIPS), pp. 2787–2795.

Bouma, G., 2009. Normalized (pointwise) mutual information in collocation extraction, in: Proceedings of the Biennial GSCL Conference 2009, pp. 31–40.

Brin, S., Page, L., 1998. The anatomy of a large-scale hypertextual web search engine. Computer networks and ISDN systems 30, 107–117.

Bryan, J., Moriano, P., 2023. Graph-based machine learning improves just-in-time defect prediction. PLOS ONE 18, e0284077. doi:10.1371/journal.pone.0284077.

Bui, N.D.Q., Yu, Y., Jiang, L., 2021. Infercode: Self-supervised learning of code representations by predicting subtrees, in: Proceedings of the 43rd International Conference on Software Engineering (ICSE), pp. 1186–1197. doi:10.1109/ICSE43902.2021.00109.

Cabral, G.G., Minku, L.L., 2023. Towards reliable online just-in-time software defect prediction. IEEE Transactions on Software Engineering 49, 1342–1358. doi:10.1109/TSE.2022.3175789.

Cai, L., Mao, X., Zhou, Y., Long, Z., Wu, C., Lan, M., 2024. A survey on temporal knowledge graph: Representation learning and applications. URL: https://arxiv.org/abs/2403.04782, arXiv:2403.04782.

Chen, X., Xia, H., Pei, W., Ni, C., Liu, K., 2023. Boosting multi-objective just-in-time software defect prediction by fusing expert metrics and semantic metrics. Journal of Systems and Software 206, 111853. doi:10.1016/j.jss.2023.111853.

Chilowicz, M., Duris, E., Roussel, G., 2009. Syntax tree fingerprinting for source code similarity detection, in: 2009 IEEE 17th international conference on program comprehension, IEEE. pp. 243–247. doi:10.1109/ICPC.2009.5090050.

Cho, Y., Kwon, J.H., Yi, J., Ko, I.Y., 2022. Extending developer experience metrics for better effort-aware just-in-time defect prediction.

IEEE Access 10, 128218–128231. doi:10.1109/ACCESS.2022.3227339.

Church, K., Hanks, P., 1990. Word association norms, mutual information, and lexicography. Computational linguistics 16, 22–29.

D'Ambros, M., Lanza, M., Robbes, R., 2012. Evaluating defect prediction approaches: a benchmark and an extensive comparison. Empirical Software Engineering 17, 531–577. doi:10.1007/s10664-011-9173-9.

Dettmers, T., Minervini, P., Stenetorp, P., Riedel, S., 2018. Convolutional 2d knowledge graph embeddings, in: Proceedings of the 32nd AAAI Conference on Artificial Intelligence (AAAI), pp. 1811–1818. doi:10.1609/aaai.v32i1.11573.

Falleri, J.R., Morandat, F., Blanc, X., Martinez, M., Monperrus, M., 2014. Fine-grained and accurate source code differencing, in: Proceedings of the 29th ACM/IEEE international conference on Automated software engineering, pp. 313–324. doi:10.1145/2642937.2642982.

Feng, Z., Guo, D., Tang, D., Duan, N., Feng, X., Gong, M., Shou, L., Qin, B., Liu, T., Jiang, D., Zhou, M., 2020. Codebert: A pre-trained model for programming and natural languages, in: Findings of the Association for Computational Linguistics: EMNLP 2020, pp. 1536–1547. doi:10.18653/v1/2020.findings-emnlp.139.

Francis, N., Green, A., Guagliardo, P., Libkin, L., Lindaaker, T., Marsault, V., Plantikow, S., Rydberg, M., Selmer, P., Taylor, A., 2018. Cypher: An evolving query language for property graphs, in: Proceedings of the 2018 International Conference on Management of Data (SIGMOD), pp. 1433–1445. doi:10.1145/3183713.3190657.

Fukushima, T., Kamei, Y., McIntosh, S., Yamashita, K., Ubayashi, N., 2014. An empirical study of just-in-time defect prediction using cross-project models, in: Proceedings of the 11th Working Conference on Mining Software Repositories (MSR), pp. 172–181. doi:10.1145/2597073.2597075.

Goel, R., Kazemi, S.M., Brubaker, M., Poupart, P., 2020. Diachronic embedding for temporal knowledge graph completion, in: Proceedings of the 34th AAAI Conference on Artificial Intelligence (AAAI), pp. 3988–3995. doi:10.1609/aaai.v34i04.5815.

Gomes Cabral, G., Minku, L., Shihab, E., Mujahid, S., 2019. Class imbalance evolution and verification latency in just-in-time software defect prediction, in: Proceedings of the 41st International Conference on Software Engineering, IEEE. pp. 666–676. doi:10.1109/ICSE.2019.00076.

Guo, D., Ren, S., Lu, S., Feng, Z., Tang, D., Liu, S., Zhou, L., Duan, N., Svyatkovskiy, A., Fu, S., Tufano, M., Deng, S.K., Clement, C., Drain, D., Sundaresan, N., Yin, J., Jiang, D., Zhou, M., 2021. Graphcodebert: Pre-training code representations with data flow, in: International Conference on Learning Representations (ICLR).

Guo, Q., Zhuang, F., Qin, C., Zhu, H., Xie, X., Xiong, H., He, Q., 2022. A survey on knowledge graph-based recommender systems. IEEE Transactions on Knowledge and Data Engineering 34, 3549–3568. doi:10.1109/TKDE.2020.3028705.

Hall, T., Beecham, S., Bowes, D., Gray, D., Counsell, S., 2012. A systematic literature review on fault prediction performance in software engineering. IEEE Transactions on Software Engineering 38, 1276–1304. doi:10.1109/TSE.2011.103.

Hassan, A.E., 2009. Predicting faults using the complexity of code changes, in: 2009 IEEE 31st international conference on software engineering, IEEE. pp. 78–88. doi:10.1109/ICSE.2009.5070510.

Haveliwala, T.H., 2002. Topic-sensitive pagerank, in: Proceedings of the 11th International Conference on World Wide Web, ACM. pp. 517–526. doi:10.1145/511446.511513.

Hellendoorn, V.J., Sutton, C., Singh, R., Maniatis, P., Bieber, D., 2020. Global relational models of source code, in: International Conference on Learning Representations (ICLR).

Hesamolhokama, M., Rohani, B., Shafiee, A., Fazli, M., Habibi, J., 2025. From illusion to insight: Change-aware file-level software defect prediction using agentic ai. URL: https://arxiv.org/abs/2512.23875, arXiv:2512.23875.

Hindle, A., Barr, E.T., Su, Z., Gabel, M., Devanbu, P., 2012. On the naturalness of software, in: Proceedings of the 34th International Conference on Software Engineering (ICSE), pp. 837–847.

Hoang, T., Dam, H.K., Kamei, Y., Lo, D., Ubayashi, N., 2019. Deepjit: An end-to-end deep learning framework for just-in-time defect prediction, in: Proceedings of the 16th International Conference on Mining Software Repositories (MSR), pp. 34–45. doi:10.1109/MSR.2019.00016.

Hoang, T., Kang, H.J., Lo, D., Lawall, J., 2020. Cc2vec: Distributed representations of code changes, in: Proceedings of the 42nd International Conference on Software Engineering (ICSE), pp. 518–529. doi:10.1145/3377811.3380361.

Hogan, A., Blomqvist, E., Cochez, M., d'Amato, C., de Melo, G., Gutierrez, C., Kirrane, S., Gayo, J.E.L., Navigli, R., Neumaier, S., Ngonga Ngomo, A.C., Polleres, A., Rashid, S.M., Rula, A., Schmelzeisen, L., Sequeda, J., Staab, S., Zimmermann, A., 2021. Knowledge graphs. ACM Computing Surveys 54, 1–37. doi:10.1145/3447772.

Ji, S., Pan, S., Cambria, E., Marttinen, P., Yu, P.S., 2022. A survey on knowledge graphs: Representation, acquisition, and applications. IEEE Transactions on Neural Networks and Learning Systems 33, 494–514. doi:10.1109/TNNLS.2021.3070843.

Jiang, Y., Shen, B., Gu, X., 2025. Just-in-time software defect prediction via bi-modal change representation learning. Journal of Systems and Software 219, 112253. doi:10.1016/j.jss.2024.112253.

Jin, W., Qu, M., Jin, X., Ren, X., 2020. Recurrent event network: Autoregressive structure inference over temporal knowledge graphs, in: Proceedings of the 2020 Conference on Empirical Methods in Natural Language Processing (EMNLP), pp. 6669–6683. doi:10.18653/v1/2020.emnlp-main.541.

Kamei, Y., Fukushima, T., McIntosh, S., Yamashita, K., Ubayashi, N., Hassan, A.E., 2016. Studying just-in-time defect prediction using cross-project models. Empirical Software Engineering 21, 2072–2106. doi:10.1007/s10664-015-9400-x.

Kamei, Y., Shihab, E., Adams, B., Hassan, A.E., Mockus, A., Sinha, A., Ubayashi, N., 2013. A large-scale empirical study of just-in-time quality assurance. IEEE Transactions on Software Engineering 39, 757–773. doi:10.1109/TSE.2012.70.

Kanade, A., Maniatis, P., Balakrishnan, G., Shi, K., 2020. Learning and evaluating contextual embedding of source code, in: Proceedings of the 37th International Conference on Machine Learning (ICML), pp. 5110–5121.

Keshavarz, H., Nagappan, M., 2022. Apachejit: a large dataset for just-in-time defect prediction, in: Proceedings of the 19th international conference on mining software repositories, pp. 191–195. doi:10.1145/3524842.3527996.

Kim, S., Whitehead, E.J., Zhang, Y., 2008. Classifying software changes: Clean or buggy? IEEE Transactions on Software Engineering 34, 181–196. doi:10.1109/TSE.2007.70773.

Kirkpatrick, J., Pascanu, R., Rabinowitz, N., Veness, J., Desjardins, G., Rusu, A.A., Milan, K., Quan, J., Ramalho, T., Grabska-Barwinska, A., Hassabis, D., Clopath, C., Kumaran, D., Hadsell, R., 2017. Overcoming catastrophic forgetting in neural networks. Proceedings of the National Academy of Sciences 114, 3521–3526. doi:10.1073/pnas.1611835114.

Kondo, M., German, D.M., Mizuno, O., Choi, E., 2020. The impact of context metrics on just-in-time defect prediction. Empirical Software Engineering 25, 890–939. doi:10.1007/s10664-019-09736-3.

Lacroix, T., Obozinski, G., Usunier, N., 2020. Tensor decompositions for temporal knowledge base completion, in: International Conference on Learning Representations (ICLR).

Lee, G., Ju, H., Lee, S.U.J., 2024. Neurojit: Improving just-in-time defect prediction using neurophysiological and empirical perceptions of modern developers, in: Proceedings of the 39th IEEE/ACM International Conference on Automated Software Engineering, pp. 594–605. doi:10.1145/3691620.3695056.

Lessmann, S., Baesens, B., Mues, C., Pietsch, S., 2008. Benchmarking classification models for software defect prediction: A proposed framework and novel findings. IEEE Transactions on Software Engineering 34, 485–496. doi:10.1109/TSE.2008.35.

Li, J., He, P., Zhu, J., Lyu, M.R., 2017. Software defect prediction via convolutional neural network, in: Proceedings of the IEEE International Conference on Software Quality, Reliability and Security (QRS), pp. 318–328. doi:10.1109/QRS.2017.42.

Li, Y., Tarlow, D., Brockschmidt, M., Zemel, R., 2016. Gated graph sequence neural networks, in: International Conference on Learning Representations (ICLR).

Lin, Y., Liu, Z., Sun, M., Liu, Y., Zhu, X., 2015. Learning entity and relation embeddings for knowledge graph completion, in: Proceedings of the 29th AAAI Conference on Artificial Intelligence (AAAI), pp. 2181–2187. doi:10.1609/aaai.v29i1.9491.

Liu, J., Ai, J., Lu, M., Wang, J., Shi, H., 2023a. Semantic feature learning for software defect prediction from source code and external knowledge. Journal of Systems and Software 204, 111753. doi:10.1016/j.jss.2023.111753.

Liu, M., Yang, Y., Lou, Y., Peng, X., Zhou, Z., Du, X., Yang, T., 2023b. Recommending analogical apis via knowledge graph embedding, in: Proceedings of the 31st ACM Joint European Software Engineering Conference and Symposium on the Foundations of Software Engineering (ESEC/FSE), pp. 1496–1508. doi:10.1145/3611643.3616305.

MacLean, F., 2021. Knowledge graphs and their applications in drug discovery. Expert Opinion on Drug Discovery 16, 1057–1069. doi:10.1080/17460441.2021.1910673.

Macskassy, S.A., Provost, F., 2003. A simple relational classifier, in: Proceedings of the Second International Workshop on Multi-Relational Data Mining, pp. 64–76.

McIntosh, S., Kamei, Y., 2018. Are fix-inducing changes a moving target? a longitudinal case study of just-in-time defect prediction. IEEE Transactions on Software Engineering 44, 412–428. doi:10.1109/TSE.2017.2693980.

Menzies, T., Greenwald, J., Frank, A., 2007. Data mining static code attributes to learn defect predictors. IEEE Transactions on Software Engineering 33, 2–13. doi:10.1109/TSE.2007.256941.

Menzies, T., Milton, Z., Turhan, B., Cukic, B., Jiang, Y., Bener, A., 2010. Defect prediction from static code features: Current results, limitations, new approaches. Automated Software Engineering 17, 375–407. doi:10.1007/s10515-010-0069-5.

Mihalcea, R., Tarau, P., 2004. Textrank: Bringing order into text, in: Proceedings of the 2004 conference on empirical methods in natural language processing, pp. 404–411.

Mikolov, T., Sutskever, I., Chen, K., Corrado, G.S., Dean, J., 2013. Distributed representations of words and phrases and their compositionality, in: Advances in Neural Information Processing Systems (NeurIPS), pp. 3111–3119.

Mockus, A., Weiss, D.M., 2000. Predicting risk of software changes. Bell Labs Technical Journal 5, 169–180. doi:10.1002/bltj.2229.

Moser, R., Pedrycz, W., Succi, G., 2008. A comparative analysis of the efficiency of change metrics and static code attributes for defect prediction, in: Proceedings of the 30th international conference on Software engineering, pp. 181–190. doi:10.1145/1368088.1368114.

Mou, L., Li, G., Zhang, L., Wang, T., Jin, Z., 2016. Convolutional neural networks over tree structures for programming language processing, in: Proceedings of the 30th AAAI Conference on Artificial Intelligence (AAAI), pp. 1287–1293. doi:10.1609/aaai.v30i1.10139.

Nagappan, N., Ball, T., 2005. Use of relative code churn measures to predict system defect density, in: Proceedings of the 27th international conference on Software engineering, pp. 284–292. doi:10.1145/1062455.1062514.

Nam, J., Pan, S.J., Kim, S., 2013. Transfer defect learning, in: Proceedings of the 35th International Conference on Software Engineering (ICSE), pp. 382–391. doi:10.1109/ICSE.2013.6606584.

Ni, C., Wang, W., Yang, K., Xia, X., Liu, K., Lo, D., 2022. The best of both worlds: Integrating semantic features with expert features for defect prediction and localization, in: Proceedings of the 30th ACM Joint European Software Engineering Conference and Symposium on the Foundations of Software Engineering (ESEC/FSE), pp. 672–683. doi:10.1145/3540250.3549165.

Nickel, M., Murphy, K., Tresp, V., Gabrilovich, E., 2016. A review of relational machine learning for knowledge graphs. Proceedings of the IEEE 104, 11–33. doi:10.1109/JPROC.2015.2483592.

Nickel, M., Tresp, V., Kriegel, H.P., 2011. A three-way model for collective learning on multi-relational data, in: Proceedings of the 28th International Conference on Machine Learning (ICML), pp. 809–816.

Pascarella, L., Palomba, F., Bacchelli, A., 2019. Fine-grained just-in-time defect prediction. Journal of Systems and Software 150, 22–36. doi:10.1016/j.jss.2018.12.001.

Perozzi, B., Al-Rfou, R., Skiena, S., 2014. Deepwalk: Online learning of social representations, in: Proceedings of the 20th ACM SIGKDD International Conference on Knowledge Discovery and Data Mining, ACM. pp. 701–710. doi:10.1145/2623330.2623732.

Pornprasit, C., Tantithamthavorn, C., 2021. Jitline: A simpler, better, faster, finer-grained just-in-time defect prediction, in: Proceedings of the 18th International Conference on Mining Software Repositories (MSR), pp. 369–379. doi:10.1109/MSR52588.2021.00049.

Pornprasit, C., Tantithamthavorn, C., Jiarpakdee, J., Fu, M., Thongtanunam, P., 2021. Pyexplainer: Explaining the predictions of just-in-time defect models, in: Proceedings of the 36th IEEE/ACM International Conference on Automated Software Engineering (ASE), pp. 407–418. doi:10.1109/ASE51524.2021.9678763.

Pornprasit, C., Tantithamthavorn, C.K., 2023. Deeplinedp: Towards a deep learning approach for line-level defect prediction. IEEE Transactions on Software Engineering 49, 84–98. doi:10.1109/TSE.2022.3144348.

Qiao, L., Wang, Y., 2019. Effort-aware and just-in-time defect prediction with neural network. PLOS ONE 14, e0211359. doi:10.1371/journal.pone.0211359.

Rivest, R.L., 1992. The MD5 message-digest algorithm. Technical Report RFC 1321. Network Working Group, IETF. doi:10.17487/RFC1321.

Rousseau, F., Vazirgiannis, M., 2013. Graph-of-word and tw-idf: new approach to ad hoc ir, in: Proceedings of the 22nd ACM international conference on Information & Knowledge Management, pp. 59–68. doi:10.1145/2505515.2505671.

Rousseau, F., Vazirgiannis, M., 2015. Main core retention on graph-of-words for single-document keyword extraction, in: European Conference on Information Retrieval, Springer. pp. 382–393. doi:10.1007/978-3-319-16354-3_42.

Sahar, H., Bangash, A.A., Hindle, A., Barbosa, D., 2024. Irjit: A simple, online, information retrieval approach for just-in-time software defect prediction. Empirical Software Engineering 29, 131.

doi:10.1007/s10664-024-10514-z.
Scarselli, F., Gori, M., Tsoi, A.C., Hagenbuchner, M., Monfardini, G., 2009. The graph neural network model. IEEE Transactions on Neural Networks 20, 61–80. doi:10.1109/TNN.2008.2005605.
Schlichtkrull, M., Kipf, T.N., Bloem, P., van den Berg, R., Titov, I., Welling, M., 2018. Modeling relational data with graph convolutional networks, in: The Semantic Web – 15th International Conference (ESWC), Springer. pp. 593–607. doi:10.1007/978-3-319-93417-4_38.
Šikić, L., Kurdija, A.S., Vladimir, K., Šilić, M., 2022. Graph neural network for source code defect prediction. IEEE access 10, 10402–10415. doi:10.1109/ACCESS.2022.3144598.
Śliwerski, J., Zimmermann, T., Zeller, A., 2005. When do changes induce fixes?, in: Proceedings of the 2005 International Workshop on Mining Software Repositories (MSR), pp. 1–5. doi:10.1145/1083142.1083147.
Song, L., Minku, L.L., 2023. A procedure to continuously evaluate predictive performance of just-in-time software defect prediction models during software development. IEEE Transactions on Software Engineering 49, 646–666. doi:10.1109/TSE.2022.3158831.
Song, L., Minku, L.L., Yao, X., 2023. On the validity of retrospective predictive performance evaluation procedures in just-in-time software defect prediction. Empirical Software Engineering 28, 124. doi:10.1007/s10664-023-10341-8.
Suchanek, F.M., Kasneci, G., Weikum, G., 2007. Yago: A core of semantic knowledge, in: Proceedings of the 16th International Conference on World Wide Web (WWW), pp. 697–706. doi:10.1145/1242572.1242667.
Sun, Z., Deng, Z.H., Nie, J.Y., Tang, J., 2019. Rotate: Knowledge graph embedding by relational rotation in complex space, in: International Conference on Learning Representations (ICLR).
Tabassum, S., Minku, L.L., Feng, D., 2023. Cross-project online just-in-time software defect prediction. IEEE Transactions on Software Engineering 49, 268–287. doi:10.1109/TSE.2022.3150153.
Tai, K.S., Socher, R., Manning, C.D., 2015. Improved semantic representations from tree-structured long short-term memory networks, in: Proceedings of the 53rd Annual Meeting of the Association for Computational Linguistics (ACL), pp. 1556–1566. doi:10.3115/v1/P15-1150.
Tan, M., Tan, L., Dara, S., Mayeux, C., 2015. Online defect prediction for imbalanced data, in: Proceedings of the 37th IEEE/ACM International Conference on Software Engineering, pp. 99–108. doi:10.1109/ICSE.2015.139.
Tantithamthavorn, C., McIntosh, S., Hassan, A.E., Matsumoto, K., 2017. An empirical comparison of model validation techniques for defect prediction models. IEEE Transactions on Software Engineering 43, 1–18. doi:10.1109/TSE.2016.2584050.
Trivedi, R., Dai, H., Wang, Y., Song, L., 2017. Know-evolve: Deep temporal reasoning for dynamic knowledge graphs, in: Proceedings of the 34th International Conference on Machine Learning (ICML), pp. 3462–3471.
Trouillon, T., Welbl, J., Riedel, S., Gaussier, E., Bouchard, G., 2016. Complex embeddings for simple link prediction, in: Proceedings of the 33rd International Conference on Machine Learning (ICML), pp. 2071–2080.
Vashishth, S., Sanyal, S., Nitin, V., Talukdar, P., 2020. Composition-based multi-relational graph convolutional networks, in: International Conference on Learning Representations (ICLR).
Vrandečić, D., Krötzsch, M., 2014. Wikidata: A free collaborative knowledgebase. Communications of the ACM 57, 78–85. doi:10.1145/2629489.
Wang, H., Zhang, F., Wang, J., Zhao, M., Li, W., Xie, X., Guo, M., 2018. Ripplenet: Propagating user preferences on the knowledge graph for recommender systems, in: Proceedings of the 27th ACM International Conference on Information and Knowledge Management (CIKM), pp. 417–426. doi:10.1145/3269206.3271739.
Wang, L., Sun, C., Zhang, C., Nie, W., Huang, K., 2023. Application of knowledge graph in software engineering field: A systematic literature review. Information and Software Technology 164, 107327.
Wang, Q., Mao, Z., Wang, B., Guo, L., 2017. Knowledge graph embedding: A survey of approaches and applications. IEEE Transactions on Knowledge and Data Engineering 29, 2724–2743. doi:10.1109/TKDE.2017.2754499.
Wang, S., Liu, T., Tan, L., 2016. Automatically learning semantic features for defect prediction, in: Proceedings of the 38th International Conference on Software Engineering (ICSE), pp. 297–308. doi:10.1145/2884781.2884804.
Wang, W., Li, G., Ma, B., Xia, X., Jin, Z., 2020. Detecting code clones with graph neural network and flow-augmented abstract syntax tree, in: Proceedings of the IEEE 27th International Conference on Software Analysis, Evolution and Reengineering (SANER), pp. 261–271. doi:10.1109/SANER48275.2020.9054857.
Wang, X., He, X., Cao, Y., Liu, M., Chua, T.S., 2019. Kgat: Knowledge graph attention network for recommendation, in: Proceedings of the 25th ACM SIGKDD International Conference on Knowledge Discovery and Data Mining (KDD), pp. 950–958. doi:10.1145/3292500.3330989.
Wang, Y., Wang, W., Joty, S., Hoi, S.C.H., 2021. Codet5: Identifier-aware unified pre-trained encoder-decoder models for code understanding and generation, in: Proceedings of the 2021 Conference on Empirical Methods in Natural Language Processing (EMNLP), pp. 8696–8708. doi:10.18653/v1/2021.emnlp-main.685.
Wang, Z., Zhang, J., Feng, J., Chen, Z., 2014. Knowledge graph embedding by translating on hyperplanes, in: Proceedings of the 28th AAAI Conference on Artificial Intelligence (AAAI), pp. 1112–1119. doi:10.1609/aaai.v28i1.8870.
Weinberger, K.Q., Dasgupta, A., Langford, J., Smola, A.J., Attenberg, J., 2009. Feature hashing for large scale multitask learning, in: Proceedings of the 26th Annual International Conference on Machine Learning, pp. 1113–1120. doi:10.1145/1553374.1553516.
Wolpert, D.H., 1992. Stacked generalization. Neural networks 5, 241–259. doi:10.1016/S0893-6080(05)80023-1.
Wu, Z., Pan, S., Chen, F., Long, G., Zhang, C., Yu, P.S., 2021. A comprehensive survey on graph neural networks. IEEE Transactions on Neural Networks and Learning Systems 32, 4–24. doi:10.1109/TNNLS.2020.2978386.
Yang, B., Yih, W.t., He, X., Gao, J., Deng, L., 2015a. Embedding entities and relations for learning and inference in knowledge bases, in: International Conference on Learning Representations (ICLR).
Yang, X., Lo, D., Xia, X., Zhang, Y., Sun, J., 2015b. Deep learning for just-in-time defect prediction, in: Proceedings of the 2015 IEEE International Conference on Software Quality, Reliability and Security (QRS), IEEE. pp. 17–26. doi:10.1109/QRS.2015.14.
Zain, Z.M., Sakri, S., Ismail, N.H.A., 2023. Application of deep learning in software defect prediction: systematic literature review and meta-analysis. Information and Software Technology 158, 107175. doi:10.1016/j.infsof.2023.107175.
Zeng, Z., Zhang, Y., Zhang, H., Zhang, L., 2021. Deep just-in-time defect prediction: How far are we?, in: Proceedings of the 30th ACM SIGSOFT International Symposium on Software Testing and Analysis (ISSTA), pp. 427–438. doi:10.1145/3460319.3464819.
Zhang, J., Wang, X., Zhang, H., Sun, H., Wang, K., Liu, X., 2019a. A novel neural source code representation based on abstract syntax tree, in: Proceedings of the 41st International Conference on Software Engineering (ICSE), pp. 783–794. doi:10.1109/ICSE.2019.00086.
Zhang, Y., Kong, X., Shen, Z., Li, J., Yi, Q., Shen, G., Dong, B.,

2024. A survey on temporal knowledge graph embedding: Models and applications. Knowledge-Based Systems 304, 112454. doi:10.1016/j.knosys.2024.112454.

Zhang, Z., Han, X., Liu, Z., Jiang, X., Sun, M., Liu, Q., 2019b. Ernie: Enhanced language representation with informative entities, in: Proceedings of the 57th Annual Meeting of the Association for Computational Linguistics (ACL), pp. 1441–1451. doi:10.18653/v1/P19-1139.

Zhao, X., Jiang, R., Han, Y., Li, A., Peng, Z., 2024. A survey on cybersecurity knowledge graph construction. Computers & Security 136, 103524. doi:10.1016/j.cose.2023.103524.

Zhao, Y., Chen, H., 2023. Deep incremental learning of imbalanced data for just-in-time software defect prediction. URL: https://arxiv.org/abs/2310.12289, arXiv:2310.12289.

Zhao, Y., Damevski, K., Chen, H., 2023. A systematic survey of just-in-time software defect prediction. ACM Computing Surveys 55, 1–35. doi:10.1145/3567550.

Zhou, C., He, P., Zeng, C., Ma, J., 2022. Software defect prediction with semantic and structural information of codes based on graph neural networks. Information and Software Technology 152, 107057. doi:10.1016/j.infsof.2022.107057.

Zhou, X., Han, D., Lo, D., 2025. Bridging expert knowledge with deep learning techniques for just-in-time defect prediction. Empirical Software Engineering 30, 1–34. doi:10.1007/s10664-024-10591-0.

Zhou, Y., Liu, S., Siow, J., Du, X., Liu, Y., 2019. Devign: Effective vulnerability identification by learning comprehensive program semantics via graph neural networks, in: Advances in Neural Information Processing Systems (NeurIPS).

Zhu, X., Ghahramani, Z., Lafferty, J., 2003. Semi-supervised learning using gaussian fields and harmonic functions, in: Proceedings of the 20th International Conference on Machine Learning (ICML), pp. 912–919.

Zimmermann, T., Nagappan, N., Gall, H., Giger, E., Murphy, B., 2009. Cross-project defect prediction: A large scale experiment on data vs. domain vs. process, in: Proceedings of the 7th Joint Meeting of the European Software Engineering Conference and the ACM SIGSOFT Symposium on the Foundations of Software Engineering (ESEC/FSE), pp. 91–100. doi:10.1145/1595696.1595713.

Appendix A. Alternative Within-File Representations

CFG, DFG, and PDG are constructed independently for each Java method using `CFGBuilder`, `DefUseBuilder`, and `CPGBuilder`, respectively. The CFG represents execution order and branching; the DFG represents definition-use value flow, and the PDG combines control and data dependencies. Table A.15 summarizes their construction. Construct coverage therefore follows the nodes produced by the respective builder.

Unlike the AST, these graphs do not have canonically ordered children or a unique parent, so subtree hashing cannot be applied directly. Their shared matcher instead ranks same-type nodes within a method by (`line`, `id`) and matches them by ordinal, with a deterministic same-type greedy pass for remaining nodes. A matched node is marked `MOVES` when its primary predecessor changes to a different predecessor type; unmatched nodes yield `ADDS` and `REMOVES`, and changed matched nodes yield `UPDATES`. If identity matching is unstable, the implementation provides a conservative typed-multiset fallback containing only additions and removals. Thus, CFG, DFG, and PDG differ in the program structure they encode, while their matching and downstream delta interface are held fixed. Figure A.17 illustrates the three representations.

Appendix B. Layer-Wise Results for Individual Inference Channels

To complement the fixed-F_{ov} analysis in Section 5.3, we report the layer-wise evaluation for the five individual graph-inference channels in Table B.16. These results are kept separate from the main analysis because the contribution of a representation is not invariant to the inference mechanism. The magnitude, and occasionally the ordering, of layer-level gains can change across inference channels and projects. The main text therefore holds inference fixed at F_{ov} when attributing performance changes to the representation.

Appendix C. Commit–Hub Projection and Graph-Based Inference

The five graph-based inference channels operate on the commit–hub projection introduced in Section 3.3.6. At commit j, this projection is a weighted bipartite graph

$$\mathcal{P}^{(j)} = \left(\mathcal{C}^{(j)} \cup \mathcal{H}^{(j)}, \mathcal{E}^{(j)}\right), \qquad \mathcal{E}^{(j)} \subseteq \mathcal{C}^{(j)} \times \mathcal{H}^{(j)}, \quad \text{(C.1)}$$

where $\mathcal{C}^{(j)}$ contains the commit nodes available at that point and $\mathcal{H}^{(j)}$ contains inference-level context hubs. Four hub types are used: `Files`, `Developers`, change tokens, and CSTG `Terms`. A hub is therefore an entity that can be shared by multiple commits and provides a path between commits with related context.

A change token is a pair (r, τ), where $r \in \{\texttt{ADDS}, \texttt{REMOVES}, \texttt{UPDATES}, \texttt{MOVES}\}$ is the structural edit operation and τ is the type of the affected `ASTNode` defined in Section 3.3.3. The AST delta of a commit is represented as a multiset of these tokens. For example, if a commit adds three `MethodInvocation` nodes, the corresponding (`ADDS`, `MethodInvocation`) token occurs three times. File and developer hubs are obtained from the Core layer, while CSTG term hubs are obtained from the semantic layer.

Table A.15: Construction and delta extraction for the alternative within-file representations.

Rep.	Builder	Nodes / edges	Matching and cycles	Validation / cost
CFG	`CFGBuilder`	Nodes are typed by control-flow `kind`; directed edges encode execution successors and branches.	Two-pass ordinal matching within each method: exact (method, type, ordinal), followed by deterministic greedy same-type matching. Cycles require no special handling because matching does not recursively traverse graph edges.	Built and matched only for affected methods using deterministic construction and matching.
DFG	`DefUseBuilder`	Definition nodes use `def_type`; use nodes are typed `USE`; edges encode definition–use value flow.	Same ordinal matcher as CFG. Multiple predecessors do not require a unique tree parent; move detection uses the primary predecessor.	Same deterministic procedure and scope as CFG.
PDG	`CPGBuilder`	Nodes are typed by `kind`; edges combine control and data dependencies.	Same ordinal matcher as CFG and DFG; no canonical child ordering is assumed.	Same deterministic procedure and scope as CFG/DFG.

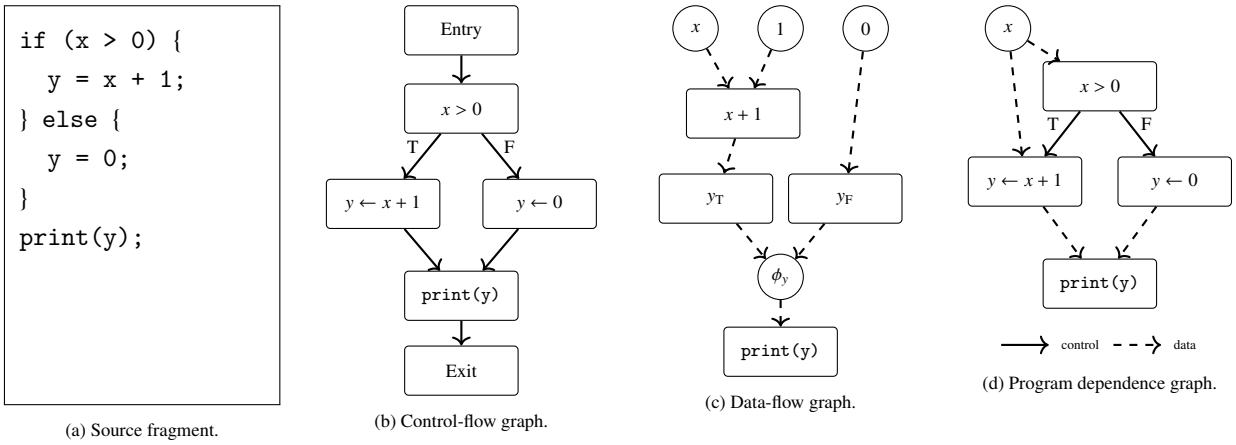

(a) Source fragment.

(b) Control-flow graph.

(c) Data-flow graph.

(d) Program dependence graph.

Figure A.17: The same conditional code fragment represented using alternative structural representations: (a) the source fragment, (b) the CFG, (c) the DFG, and (d) the PDG. In the PDG, solid edges denote control dependencies, whereas dashed edges denote data dependencies.

Table B.16: Layer-wise online performance of the five individual graph-inference channels across all 11 projects. Underlining marks the best representation within each inference row.

Project	Inf.	Layer 1			Layer 2: within-file subgraph												Layer 3		
		Core			+AST			+CFG			+DFG			+PDG			CSTG		
		F_1	G	AUC	F_1	G	AUC	F_1	G	AUC	F_1	G	AUC	F_1	G	AUC	F_1	G	AUC
ActiveMQ	RN	.483	.563	.675	.340	.389	.555	.433	.509	.593	.432	.508	.614	.435	.511	.592	.348	.401	.561
	PPR	.532	.604	.671	.589	.663	.704	.569	.646	.699	.571	.647	.696	.573	.648	.700	.660	.702	.778
	LP	.442	.519	.650	.294	.318	.575	.349	.400	.606	.350	.402	.614	.341	.389	.606	.437	.514	.670
	DW	.505	.573	.602	.579	.629	.682	.547	.612	.648	.537	.606	.636	.544	.607	.646	.609	.665	.711
	KGE	.530	.593	.624	.583	.651	.701	.527	.603	.639	.516	.592	.644	.528	.607	.653	.616	.670	.719
Camel	RN	.588	.648	.706	.371	.524	.626	.435	.595	.663	.473	.632	.683	.433	.593	.662	.379	.533	.629
	PPR	.535	.654	.696	.508	.648	.687	.522	.664	.690	.528	.665	.693	.519	.660	.689	.635	.715	.772
	LP	.458	.607	.664	.181	.245	.553	.360	.512	.613	.395	.553	.625	.360	.511	.613	.471	.634	.654
	DW	.478	.570	.608	.554	.635	.697	.514	.621	.662	.510	.612	.646	.530	.626	.667	.569	.669	.718
	KGE	.464	.596	.624	.558	.661	.705	.485	.620	.645	.516	.642	.673	.506	.631	.658	.590	.689	.748
Cassandra	RN	.389	.330	.621	.396	.338	.570	.459	.434	.609	.429	.392	.609	.455	.428	.606	.405	.352	.577
	PPR	.489	.481	.635	.563	.571	.668	.525	.525	.657	.532	.534	.658	.526	.526	.657	.610	.621	.737
	LP	.331	.221	.560	.327	.212	.505	.328	.214	.523	.328	.214	.515	.328	.214	.523	.327	.212	.599
	DW	.589	.602	.662	.611	.625	.671	.613	.626	.667	.572	.584	.641	.612	.626	.670	.629	.643	.704
	KGE	.479	.471	.596	.597	.610	.672	.555	.562	.621	.530	.534	.592	.527	.530	.598	.643	.657	.697
Flink	RN	.581	.649	.731	.389	.431	.546	.406	.453	.570	.406	.454	.562	.406	.454	.570	.391	.434	.554
	PPR	.646	.660	.755	.622	.679	.722	.626	.682	.715	.620	.679	.714	.620	.680	.715	.715	.740	.800
	LP	.459	.521	.622	.349	.373	.550	.379	.417	.577	.367	.400	.573	.379	.417	.577	.363	.394	.625
	DW	.555	.610	.658	.590	.639	.696	.602	.645	.688	.581	.629	.673	.603	.645	.689	.578	.642	.731
	KGE	.506	.568	.602	.629	.666	.721	.562	.605	.639	.506	.569	.603	.534	.593	.626	.645	.685	.759
Groovy	RN	.519	.614	.709	.365	.445	.650	.426	.520	.651	.446	.542	.666	.420	.512	.648	.376	.458	.658
	PPR	.593	.668	.726	.595	.676	.717	.596	.681	.730	.622	.686	.729	.597	.683	.729	.674	.707	.781
	LP	.469	.566	.698	.342	.414	.654	.382	.466	.673	.390	.476	.672	.388	.474	.672	.486	.589	.714
	DW	.548	.600	.650	.571	.641	.688	.558	.630	.672	.551	.618	.655	.554	.629	.673	.619	.673	.731
	KGE	.487	.577	.634	.610	.678	.718	.570	.641	.679	.530	.608	.665	.543	.618	.647	.626	.672	.725
HBase	RN	.381	.271	.619	.364	.230	.559	.452	.387	.592	.467	.409	.586	.449	.383	.590	.377	.257	.565
	PPR	.488	.445	.658	.547	.522	.676	.574	.560	.680	.583	.572	.675	.579	.566	.679	.682	.684	.764
	LP	.377	.268	.554	.360	.225	.493	.363	.232	.518	.363	.232	.515	.363	.232	.517	.368	.243	.587
	DW	.560	.544	.632	.648	.650	.685	.623	.623	.655	.592	.587	.620	.619	.618	.651	.651	.654	.694
	KGE	.475	.435	.604	.634	.633	.702	.578	.568	.652	.578	.567	.639	.554	.537	.629	.637	.637	.722
Hive	RN	.475	.315	.655	.445	.258	.652	.487	.333	.676	.514	.378	.678	.508	.370	.674	.443	.252	.657
	PPR	.467	.314	.639	.454	.295	.637	.444	.274	.642	.456	.298	.644	.446	.278	.642	.599	.520	.754
	LP	.465	.291	.638	.383	.049	.520	.398	.127	.593	.401	.138	.572	.399	.132	.593	.494	.342	.679
	DW	.447	.267	.663	.606	.551	.671	.565	.477	.653	.499	.365	.656	.545	.445	.650	.624	.567	.677
	KGE	.403	.155	.585	.536	.426	.640	.494	.353	.606	.493	.356	.607	.486	.341	.576	.576	.490	.694
Kafka	RN	.533	.494	.689	.464	.395	.677	.539	.500	.712	.570	.540	.711	.548	.513	.709	.465	.396	.689
	PPR	.428	.373	.644	.535	.509	.669	.530	.505	.671	.528	.502	.669	.511	.478	.673	.681	.679	.803
	LP	.569	.546	.665	.438	.354	.595	.512	.463	.639	.522	.476	.640	.516	.469	.642	.652	.639	.753
	DW	.621	.616	.719	.682	.684	.726	.706	.709	.729	.687	.689	.726	.705	.708	.730	.698	.700	.748
	KGE	.487	.446	.594	.591	.573	.602	.532	.503	.564	.547	.519	.604	.576	.556	.601	.664	.662	.675
Spark	RN	.415	.379	.545	.338	.214	.581	.364	.273	.567	.365	.279	.534	.370	.285	.565	.337	.214	.589
	PPR	.402	.324	.612	.361	.246	.566	.382	.283	.573	.374	.276	.558	.398	.312	.571	.540	.520	.699
	LP	.375	.330	.503	.356	.269	.509	.372	.319	.514	.371	.326	.499	.369	.314	.510	.374	.304	.577
	DW	.432	.370	.564	.488	.464	.602	.372	.285	.539	.372	.290	.546	.376	.283	.546	.490	.464	.606
	KGE	.348	.254	.486	.462	.425	.599	.508	.491	.583	.429	.382	.531	.432	.387	.549	.496	.481	.593
Zeppelin	RN	.535	.514	.569	.542	.519	.543	.542	.519	.541	.544	.522	.518	.542	.519	.540	.543	.520	.548
	PPR	.499	.471	.588	.582	.572	.648	.565	.547	.660	.570	.553	.640	.566	.548	.652	.625	.619	.688
	LP	.542	.519	.525	.543	.520	.517	.542	.519	.519	.541	.518	.510	.541	.518	.517	.541	.519	.573
	DW	.480	.472	.568	.514	.509	.610	.578	.573	.631	.547	.540	.606	.581	.577	.621	.527	.514	.627
	KGE	.531	.504	.597	.609	.603	.660	.549	.525	.615	.532	.500	.615	.566	.539	.658	.589	.586	.608
Zookeeper	RN	.424	.420	.567	.429	.373	.475	.456	.418	.524	.457	.420	.558	.455	.415	.520	.445	.399	.497
	PPR	.443	.448	.588	.491	.492	.560	.430	.417	.532	.404	.381	.511	.416	.395	.530	.655	.665	.756
	LP	.397	.382	.561	.390	.367	.401	.393	.371	.429	.393	.371	.440	.393	.371	.429	.395	.375	.518
	DW	.338	.254	.592	.487	.475	.640	.377	.329	.543	.363	.314	.523	.375	.327	.545	.605	.616	.653
	KGE	.385	.332	.512	.552	.544	.545	.503	.489	.537	.462	.436	.521	.518	.507	.572	.616	.626	.625

Two commits that share a hub are connected through the path $c_i \to h \to c_k$ in $\mathcal{P}^{(j)}$. We call this one commit-to-commit hop, which corresponds to two edges in the bipartite projection. Two commit-to-commit hops therefore correspond to four bipartite edges. Relations that are present in the full knowledge graph but do not form commit–hub links, such as `AST_CHILD`, commit ancestry, `COOCCURS`, and file-to-file `IMPORTS`, are not edges of this projection.

Only labels that have become available under the gap constraint are used during inference. As defined in Section 3.2.2, let C_{past} denote these gap-resolved commits. For a commit c and hub h, let $\text{tf}(c, h)$ denote the number of observed occurrences of h in c. The commit–hub incidence weight is

$$W_{ch} = \text{tf}(c, h) \log\left(1 + \frac{|C_{\text{past}}|}{\text{df}_{\text{past}}(h)}\right), \tag{C.2}$$

where $\text{df}_{\text{past}}(h)$ is the number of gap-resolved past commits connected to h. The first term reflects how strongly a hub occurs in the current commit, while the logarithmic term reduces the influence of hubs that occur in many previous commits.

Let W denote the resulting weighted commit–hub incidence matrix. The adjacency matrix of the bipartite projection is

$$A_{\mathcal{P}} = \begin{bmatrix} 0 & W \\ W^\top & 0 \end{bmatrix}, \tag{C.3}$$

and its column-normalized transition matrix is

$$P = A_{\mathcal{P}} \operatorname{diag}\left(A_{\mathcal{P}}^\top \mathbf{1}\right)^\dagger, \tag{C.4}$$

where † denotes the element-wise reciprocal with zero entries kept at zero.

Although RN, LP, PPR, DW, and KGE all use this same projection, they use it in different ways. RN performs a weighted vote from commits connected through shared hubs (Macskassy and Provost, 2003). LP performs three commit–hub–commit propagation rounds and re-clamps the labels in C_{past} after every round (Zhu et al., 2003). PPR performs class-seeded propagation separately for buggy and clean commits over 40 bipartite edges (Haveliwala, 2002).

DW and KGE use the same projection but learn a representation from it rather than repeatedly following explicit paths at prediction time. DW applies truncated SVD to a positive-PMI transformation of the past commit–hub incidence matrix (Perozzi et al., 2014). KGE represents projected edges as typed triples (c, r, h) and learns DistMult embeddings (Yang et al., 2015a). The relation r distinguishes structural-token, file, developer, and CSTG-term hubs. These two methods can therefore capture patterns beyond a single shared hub through their learned representations.

Table C.17: Inference scope of the five graph-based channels on the commit–hub projection.

Method	Mechanism	Explicit reach
RN	Weighted shared-hub vote	2 edges (1 hop)
LP	Clamped label diffusion	6 edges (3 hops)
PPR	Class-seeded personalized PageRank	40 edges ($\leq$ 20 hops)
DW	PPMI matrix factorization	2 edges + global SVD
KGE	DistMult over commit–hub triples	1 edge + global embedding

Appendix D. CSTG Semantic Channel Features

The feature-based G channel uses the semantic information constructed by the CSTG layer in Section 3.3.4. Unlike the five graph-based channels, it does not produce its score from the commit–hub projection. Instead, it combines the textual-risk, term-type, intent, structural consistency, and hashed-text information of the current commit into a single feature vector and learns a commit-level defect probability.

For a commit c, let $\rho(c)$ denote the propagated textual-risk prior defined in Section 3.3.4. The five semantic-mass features are

$$\begin{aligned}\mathbf{M}(c) = [&M_{\text{code}}(c), M_{\text{bug}}(c), M_{\text{action}}(c),\\ &M_{\text{error}}(c), M_{\text{natural-language}}(c)].\end{aligned} \tag{D.1}$$

where each component gives the CSTG mass assigned to the corresponding term type. The intent assigned to the commit is represented by an indicator vector

$$\mathbf{i}(c) \in \{0, 1\}^7, \tag{D.2}$$

whose dimensions correspond to {FIX, FEAT, REFACTOR, TEST, DOCS, PERF, REVERT}. A commit assigned the OTHER intent receives the all-zero vector.

In addition to the intent label itself, we use seven features that compare the stated intent of the commit with the size and structure of its actual change. Let

$$\mathbf{q}(c) = [q_1(c), \ldots, q_7(c)] \tag{D.3}$$

Table D.18: Intent realization and cross-modal consistency features used by the CSTG semantic channel. $\mathbb{I}[\cdot]$ denotes the indicator function, $|\delta_c|$ is the size of the structural delta, and a_c and r_c denote the numbers of additions and removals, respectively.

Feature	Definition
Small-change mismatch	$q_1 = \mathbb{I}[\text{minor/trivial/typo}] \log(1 + \lvert\delta_c\rvert)$
Refactor add/remove	$q_2 = \mathbb{I}[\text{intent}(c) = \textsc{refactor}] \dfrac{a_c + r_c}{\lvert\delta_c\rvert + 1}$
Fix size	$q_3 = \mathbb{I}[\text{intent}(c) = \textsc{fix}] \log(1 + \lvert\delta_c\rvert)$
Feature without additions	$q_4 = \mathbb{I}[\text{intent}(c) = \textsc{feat}] \left(1 - \dfrac{a_c}{\lvert\delta_c\rvert + 1}\right)$
Terse large change	$q_5 = \mathbb{I}[\lvert\text{words}(c)\rvert \le 4] \log(1 + la_c + ld_c)$
Grounding gap	$q_6 = \log(1 + \lvert\text{codeTerms}(c)\rvert) - \log(1 + \lvert\delta_c\rvert)$
Revert	$q_7 = \mathbb{I}[\text{intent}(c) = \textsc{revert}]$

denote this intent-realization block. The seven features are defined in Table D.18.

Finally, let

$$\mathbf{h}(c) \in \mathbb{R}^{2^{18}} \tag{D.4}$$

denote the sparse hashed-text representation of the commit. Each typed CSTG term is converted to a tagged token and mapped to one of 2^{18} feature positions using feature hashing (Weinberger et al., 2009). The term weights computed by CSTG are carried into this representation, so terms with greater semantic weight contribute more strongly.

The complete input to the semantic channel is

$$\mathbf{z}_c = [\rho(c), \mathbf{M}(c), \mathbf{i}(c), \mathbf{q}(c), \mathbf{h}(c)]. \tag{D.5}$$

A class-balanced logistic-regression model is fitted using the currently available commits in C_{past}. The semantic-channel score is

$$G(c) = \sigma\left(\beta_0 + \boldsymbol{\beta}^\top \mathbf{z}_c\right). \tag{D.6}$$

Thus, $G(c)$ is a single commit-level probability summarizing the semantic evidence extracted by CSTG and is passed to the common score-fusion model.

Appendix E. Traversal and Global-Context Features

The commit–hub projection in Appendix C gives the five graph-based inference methods a compact representation of each commit. However, not every relation stored in KG-Commit appears in this projection. In particular, the file-to-file `IMPORTS` relations and package relationships remain in the full knowledge graph. We use a traversal/global-context (TGC) feature block to make a small part of this information available to the predictor without running the graph-based inference methods directly over the full graph.

For a target commit $c = c^{(j)}$, let $\mathcal{F}_0(c)$ denote the set of files touched by the commit. These are the files connected to c through the file-change relations in the Core layer, including `ADDED`, `MODIFIED`, `DELETED`, `RENAMED_FROM`, and `RENAMED_TO`. We use this set as the starting point for TGC. The corresponding feature block is denoted by $\mathbf{T}_0(c)$ and provides the reference information for the files directly involved in the change.

To obtain cross-file context, consider the file-level import graph available at commit j,

$$\mathcal{D}^{(j)} = \left(\mathcal{F}^{(j)}, \mathcal{I}^{(j)}\right), \tag{E.1}$$

where $\mathcal{F}^{(j)}$ is the set of files and

$$(f_a, f_b) \in \mathcal{I}^{(j)} \iff f_a \xrightarrow{\texttt{IMPORTS}} f_b \text{ in } \mathcal{K}^{(j)}. \tag{E.2}$$

The direction of this relation is important. If a touched file imports another file, the second file is an *importee*; if another file imports a touched file, that file is an *importer*. We therefore define the two one-hop sets

$$\mathcal{F}_1^{\rightarrow}(c) = \left\{f' \notin \mathcal{F}_0(c) \;\middle|\; \exists f \in \mathcal{F}_0(c) : (f, f') \in \mathcal{I}^{(j)}\right\}, \tag{E.3}$$

$$\mathcal{F}_1^{\leftarrow}(c) = \left\{f' \notin \mathcal{F}_0(c) \;\middle|\; \exists f \in \mathcal{F}_0(c) : (f', f) \in \mathcal{I}^{(j)}\right\}. \tag{E.4}$$

Thus, $\mathcal{F}_1^{\rightarrow}(c)$ contains untouched files imported by the changed files, whereas $\mathcal{F}_1^{\leftarrow}(c)$ contains untouched files that import the changed files. TGC keeps these two directions separate rather than merging them into a single neighborhood. Their features form the two direction-specific blocks $\mathbf{T}_{1,\text{dep}}(c)$ and $\mathbf{T}_{1,\text{dry}}(c)$.

This distinction allows TGC to use information that the commit–hub projection does not directly contain. Suppose, for example, that commit c changes file f, while an untouched file f' still imports f. The projection describes c through its file, developer, structural-token, and CSTG-term hubs, but it does not contain the edge $f' \xrightarrow{\texttt{IMPORTS}} f$. The incoming dependency neighborhood therefore brings f' into the context of c even though f' itself was not changed. The same applies in the other direction when a changed file depends on an untouched file.

TGC also includes package-level context. Let $\text{pkg}(f)$ denote the package containing file f. We define

$$\mathcal{F}_P(c) = \{f' \notin \mathcal{F}_0(c) \mid \exists f \in \mathcal{F}_0(c) : \text{pkg}(f') = \text{pkg}(f)\}. \tag{E.5}$$

The corresponding block $\mathbf{T}_P(c)$ therefore describes untouched files that belong to the same package as at least

one file changed by the commit. This supplies package-level context even when no direct `IMPORTS` relation exists between the two files.

Finally, TGC records where the relevant files lie in the project dependency graph. We compute PageRank and k-core values on the file-level dependency graph $\mathcal{D}^{(j)}$. PageRank measures the relative centrality of a file in the import structure, while its k-core value indicates whether it belongs to a more densely connected part of that graph. These graph-position features form $\mathbf{M}_1(c)$.

Combining the five feature groups gives

$$\mathbf{T}(c) = \left[\mathbf{T}_0(c), \mathbf{T}_{1,\text{dep}}(c), \mathbf{T}_{1,\text{dry}}(c), \mathbf{T}_P(c), \mathbf{M}_1(c)\right]. \tag{E.6}$$

Their roles are summarized in Table E.19.

Table E.19: Feature groups used by the TGC representation.

Group	Graph information used
$\mathbf{T}_0(c)$	Files directly changed by the target commit.
$\mathbf{T}_{1,\text{dep}}(c)$, $\mathbf{T}_{1,\text{dry}}(c)$	Untouched one-hop import neighbors of the changed files, with importers and importees kept as separate directions.
$\mathbf{T}_P(c)$	Untouched files in the same package as the changed files.
$\mathbf{M}_1(c)$	Position of the file context in the project dependency graph, represented through PageRank and k-core.

Because projects differ in size and dependency structure, the same raw feature value can have a different scale from one project to another. Each scalar TGC feature is therefore supplied in both raw and standardized forms. For a feature $x(c)$,

$$z_x(c) = \frac{x(c) - \mu_x^{(j)}}{\sigma_x^{(j)}}, \tag{E.7}$$

where $\mu_x^{(j)}$ and $\sigma_x^{(j)}$ are the running mean and standard deviation of that feature in the current project. The model therefore sees both the original value and how large or small it is relative to the project observed so far.

TGC augments the graph and semantic inference outputs rather than replacing them. Let $s_m(c)$ be the score of graph channel m and let $G(c)$ be the semantic-channel score defined in Appendix D. The complete $F + G + T$ model is

$$\widehat{y}(c) = \sigma\left(\theta_0 + \sum_{m \in F} \theta_m s_m(c) + \theta_G G(c) + \boldsymbol{\theta}_T^\top \mathbf{T}(c)\right). \tag{E.8}$$

The F configuration uses the selected graph-channel scores, G evaluates the semantic channel alone, $F + G$ combines the graph and semantic scores, and $F + G + T$ additionally includes the TGC feature block. As with the other learned components, fitting uses only the gap-resolved commits in C_{past}. The TGC-augmented stacking head uses standardized, class-balanced logistic regression with an L_1 penalty, $C = 0.2$, and the `liblinear` solver.

The additional context does not require a full KG traversal every time a commit is scored. The TGC information is extracted for each project and cached, and per-commit scoring reads the corresponding feature values from this cache. TGC can therefore add dependency, package, and architectural context without placing a Neo4j traversal on the online prediction path.